5-2014

Low Pressure Chemical Vapor Deposition of Semiconducting Boron Carbide Thin Films on Silicon

Thomas Gregory Wulz
University of Tennessee - Knoxville, twulz@utk.edu

To the Graduate Council:

I am submitting herewith a thesis written by Thomas Gregory Wulz entitled "Low Pressure Chemical Vapor Deposition of Semiconducting Boron Carbide Thin Films on Silicon." I have examined the final electronic copy of this thesis for form and content and recommend that it be accepted in partial fulfillment of the requirements for the degree of Master of Science, with a major in Nuclear Engineering.

Eric D. Lukosi, Major Professor

We have read this thesis and recommend its acceptance:

Howard L. Hall, Laurence F. Miller

Accepted for the Council:
Carolyn R. Hodges

Vice Provost and Dean of the Graduate School

(Original signatures are on file with official student records.)

Low Pressure Chemical Vapor Deposition of Semiconducting Boron Carbide Thin Films on Silicon

A Thesis Presented for the
Master of Science
Degree
The University of Tennessee, Knoxville

Thomas Gregory Wulz
May 2014

Dedication

To all of my family and to my loving fiancé: thank you for your patience and support.

Acknowledgements

Thank you very much to Dr. Eric Lukosi for his support and guidance during my graduate education. Thank you to Dr. Ashley Stowe of Y-12 National Security Complex for granting me use of his laboratory equipment and for facilitating in the data acquisition process in his lab. Finally, thank you to Dr. John Dunlap for his wonderful training and assistance on the electron microscopes.

Abstract

Boron carbide thin films were grown on the (100) plane of n-type silicon in a low pressure chemical vapor deposition (CVD) system from the thermal decomposition of boron trichloride and methane reactant gases with hydrogen as a carrier gas. Boron trichloride to methane molar ratio was 5, while the boron trichloride to hydrogen molar ratio was 3.5. Thin film deposition was carried out at 900 degrees Celsius at 25 Torr. The thin films were analyzed using scanning electron microscopy (SEM), transmission electron microscopy (TEM), Energy Dispersive X-Ray Spectroscopy (EDS), Laser Induced Breakdown Spectroscopy (LIBS), and current-voltage characteristics. The crystallography of the boron carbide films were determined to be largely amorphous with some polycrystalline regions. One sample was analyzed via LIBS to have a boron to carbon ratio of approximately 2. The current-voltage characteristics of another sample were Ohmic in behavior with a resistance of 300 kiliOhms. These Ohmic characteristics were hypothesized to be caused by boron carbide deposition on both sides of the silicon wafer, which created a p-n-p heterostructure. The orientation of the silicon substrate during growth caused boron carbide deposition to occur on both sides of the wafers.

Table of Contents

List of Figures

Chapter 1: Introduction

1.1 Background

Boron carbide has been used as a neutron absorber in the nuclear industry for several decades because of its high melting point, low density, and the high thermal neutron capture cross section of the ^{10}B isotope. Boron carbide is also used in bullet piercing-resistant armor worn by infantry [1], coating of wear-resistant tools, and is a grit abrasive. Boron carbide has a rhombohedral crystal structure and contains three molecules of B_4C to a unit cell [2]. The phase diagram of boron carbide suggests that a wide homogeneity range exists with carbon concentrations ranging from 9-20 at.%. Since CVD growth mechanisms often occur far from equilibrium conditions, the homogeneity range of CVD-prepared boron carbides have varied considerably, with carbon concentrations ranging from 5-50 at.% [3, 4]. Both the electrical and mechanical properties of the deposited boron carbide are affected by the relative boron and carbon concentrations within the film. The rhombohedral crystalline structure of B_4C is shown in Figure 1.

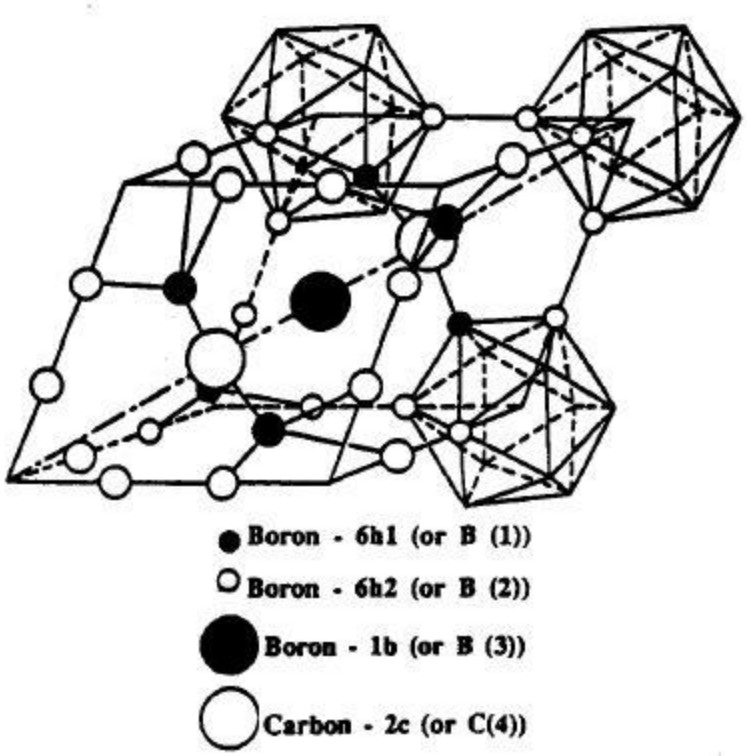

Figure 1: Rhombohedral Crystalline Structure of Boron Carbide [5]

1.2 Theory

The electrical properties of boron carbide make it an attractive material for use in the semiconductor industry, particularly in the field of solid state radiation detectors. Solid state neutron detection has higher intrinsic efficiency than current gas-filled detectors, such as helium-3 and boron trifluoride neutron detectors, due to the higher density of the sensing medium. However, in order for the radiation sensing device to achieve high detection efficiency, the boron carbide must be single crystalline and of high purity [6]. The growth of single crystalline boron carbide has been well studied [7-11], and a thorough literature review of boron carbide growth was written by Francois Thevenot in 1990 [12]. In addition, the University of Nebraska at

Lincoln has studied the fabrication of diodes consisting of CVD-grown boron carbide on n-type silicon [10, 13-15].

1.2.1 Semiconductor Theory

Since boron carbide has an excess of electron acceptor sites in the bulk material, contributed from the boron, it is considered a p-type semiconducting material. Although the band gap of boron carbide varies with carbon concentration, it is considered a wide band gap semiconductor, with a band gap of 0.77-1.80 eV for B:C of 2.4-50 [10]. A neutron sensitive, radiation detection device can be fabricated using p-type boron carbide deposited on top of an n-type semiconducting material by utilizing the physics of the p-n heterojunction. When an electric bias is applied to the boron carbide/silicon p-n heterojunction, a space charge region that is depleted of negatively charged electrons and positively charged electron-holes is created. This is due to the force from the electric field on the electrons and holes [16]. The space charge region of length W can be seen in Figure 2.

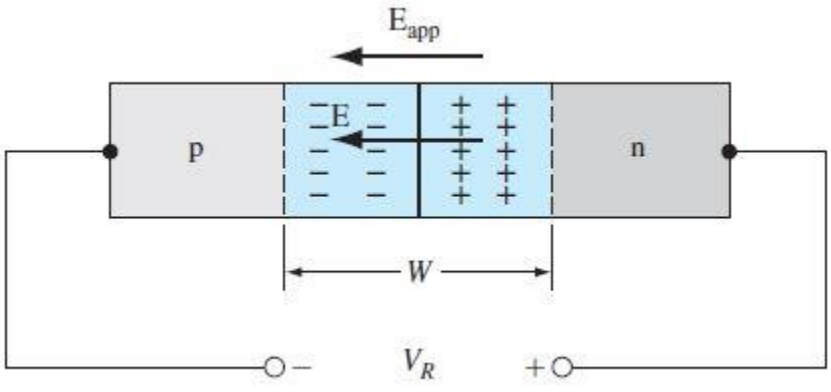

Figure 2: A P-N Junction with Applied Reverse Bias [16]

As radiation particles interact and deposit kinetic energy within this space charge region, also called the depletion region, they create electron-hole pairs, due to ionization of the sensing medium. Thermalized neutrons interact with the boron-10 isotope in boron carbide via a neutron capture reaction, which has a cross section of 3480 barns and is shown below.

$$^{10}_{5}B + ^{1}_{0}n \rightarrow ^{7}_{3}Li(0.8\ MeV) + ^{4}_{2}He(1.47\ MeV)$$

The charged particles liberated by the alpha and lithium ions can then be collected at the anode and cathode with an applied electric field, creating a pulse of electrical current. A schematic of the boron carbide-silicon radiation sensing device is shown in Figure 3, where V_{bi} is the built-in potential of the device in volts and V_a is the applied reverse bias in volts.

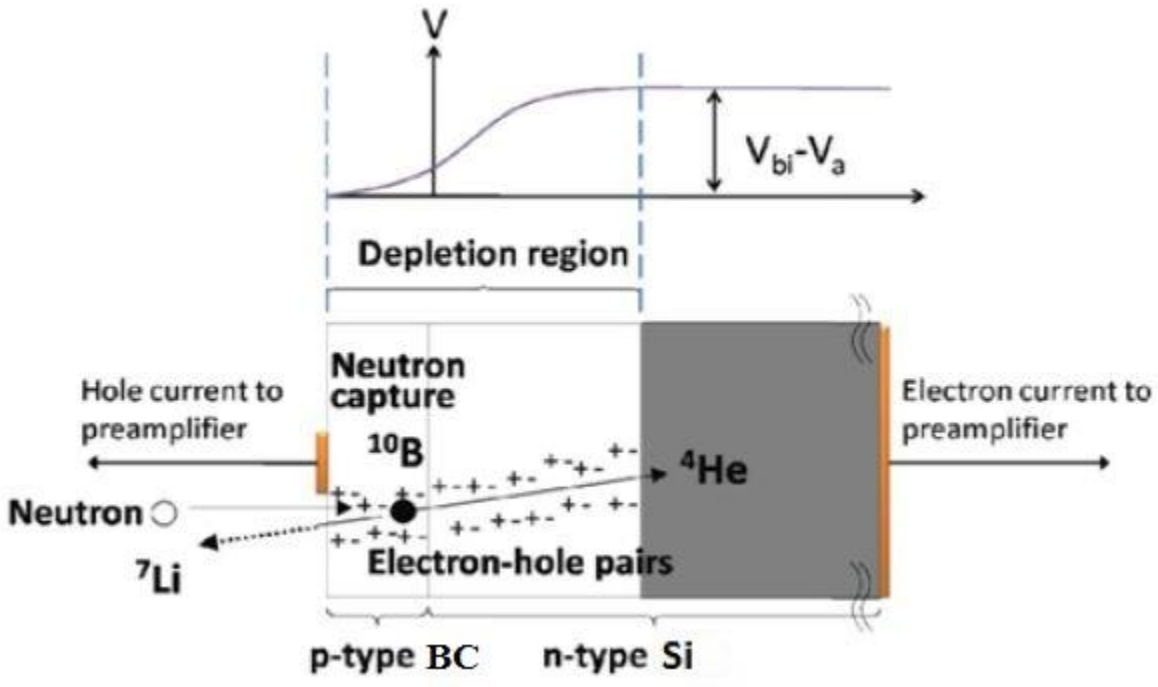

Figure 3: BC-Si Neutron Sensing Device Structure [17]

When constructing a p-n heterojunction, one must consider the epitaxy between the substrate and the deposited material. Epitaxy describes the crystalline orientation of the deposited film relative to the crystalline orientation of the growth substrate. Thus, the atomic lattice constant for each material must be considered when deciding upon a growth substrate. For a p-n heterojunction device to function properly, the lattice mismatch between the two materials should less than 5% to reduce the number of interface states [16]. The lattice constant of high purity and well-characterized rhombohedral boron carbide with carbon concentrations ranging from 7.7-20.5 at.% has been experimentally measured by Aselage *et al* to be around 5.62 Angstroms [18], while the lattice constant of the (100) plane in silicon is around 5.43 Angstroms. This yields a lattice mismatch of about 3.5%, which is within the commonly acceptable range. Thus, the (100) plane of silicon is chosen as the growth substrate for boron carbide deposition.

1.2.2 Detector Interaction Theory

The radiation detection efficiency of the device will also depend on the thickness of the deposited boron carbide films. This is due to the range of the neutron within the boron carbide material, also called the neutron mean free path. The mean free path of a neutron within a material can be expressed with the following equation:

$$\boldsymbol{mean\ free\ path} = \frac{\boldsymbol{M}}{\boldsymbol{\rho N_A \sigma}}$$

where the ***mean free path*** is in centimeters, $\boldsymbol{M}$ is the molecular weight in g/mole, $\boldsymbol{\rho}$ is the density of the material in g/cm^3, $\boldsymbol{N_A}$ is Avogadro's Number in atoms/mole, and $\boldsymbol{\sigma}$ is the interaction cross section in cm^2. Using a molecular weight of 55.3 g/mole, a density of 2.52 g/cm^3, Avogadro's

Number equal to 6.02×10^{23} atoms/mole, and an interaction cross section of 3.840×10^{-21} cm^2, the mean free path of a 0.025 eV neutron in B_4C with the boron consisting of 99% boron-10 is about 24 micrometers. Thus, to effectively stop 10% of a thermal neutron flux incident on the boron carbide, the layer would have to be about 2.4 micrometers thick.

The range of the secondary particles generated by the neutron capture reaction must also be considered. For maximum ionization in the detection region and hence maximum signal, the neutron will interact in the middle of the space charge region, where the helium-4 and lithium-7 ions will be released isotropically. Charged particles ionize materials as they interact and deposit energy. It is ideal for the secondary charged particles to deposit the majority of their energy in the depletion region because the collection of electron-hole pairs liberated by this energy deposition will create the current pulse indicative of a detection event. The distance that these ions travel within the boron carbide can be calculated with a program called TRIM, which stands for Transport of Ions in Matter [19]. TRIM uses a Monte Carlo simulation of ions interacting with materials utilizing detailed calculations of the energy transferred to target atoms at each collision. Using a boron carbide density of 2.52 g/cm^3, the 0.8 MeV lithium-7 ion and 1.47 MeV helium-4 ion will travel 1.69 μm and 3.34 μm, respectively, in B_4C. With a 12 micrometer layer of single crystalline boron carbide grown epitaxially onto n-type silicon, full charge collection of the electron-hole pairs generated by secondary charged particles from neutron capture reactions can occur, assuming the layer is semiconducting and fully depleted.

1.2.3 Chemical Vapor Deposition Theory

Chemical vapor deposition (CVD) is a very complex deposition process due to the numerous phenomena occurring at the surface of the growth substrate, including diffusion of free

radicals, forced and free convection, and nucleation from reactions. Many different classes of CVD systems exist, each with their own advantages and disadvantages. CVD processes can occur at atmospheric pressure (APCVD), reduced pressures (LPCVD), in a plasma environment (PECVD), and with Cold and Hot Wall growth conditions. Only cold and hot wall LPCVD techniques were examined.

In a cold walled CVD system, only the growth substrate is heated to elevated temperatures in order to minimize gas phase reactions on non-substrate surfaces. This allows for higher growth rates of films when compared to hot walled CVD systems. The substrate, or substrate holder, is often externally heated by an RF generator. The walls of the reactor are also actively cooled, usually with water, to further minimize film deposition on the reactor walls. In a hot walled CVD system, both the substrate and the reactor walls are heated to the same temperature by a furnace surrounding the reactor. Hot walled CVD systems also introduce the risk of contamination through chemical reactions between the reactor wall and gas vapors.

CVD processes utilize several different reaction mechanisms to induce deposition of the film. Thermal decomposition reactions, also called pyrolytic reactions, occur when the reactant gas is heated to a temperature high enough to dissociate the compound into its constituent elements. The constituent elements adsorb to the surface of the substrate, where they ideally react to form the desired compound. Reduction reactions reduce a gaseous compound into a solid through favorable reactions at high temperatures. Disproportionation and displacement reactions are two other kinds of CVD reactions. These involve typical AB + CD = AC + BD chemical reactions.

1.3 Literature Review

1.3.1 APCVD of Boron Carbide on Graphite

In 1985, Vandenbulcke *et al* grew thin films of boron carbide in a cold walled CVD system [20]. The system used a stagnation flow technique at atmospheric pressure with BCl_3 and CH_4 as the reactant gases in a H_2 carrier gas in the temperature range of 1400-2000 K. Continuous and homogenous layers of various structures of boron carbide, including B_4C, $B_{50}C_2$, $B_{13}C_3$, were deposited onto a graphite substrate that was externally heated by a RF generator. The experimental setup can be seen in Figure 4. A closer view of the substrate and deposition surface can be seen in Figure 5.

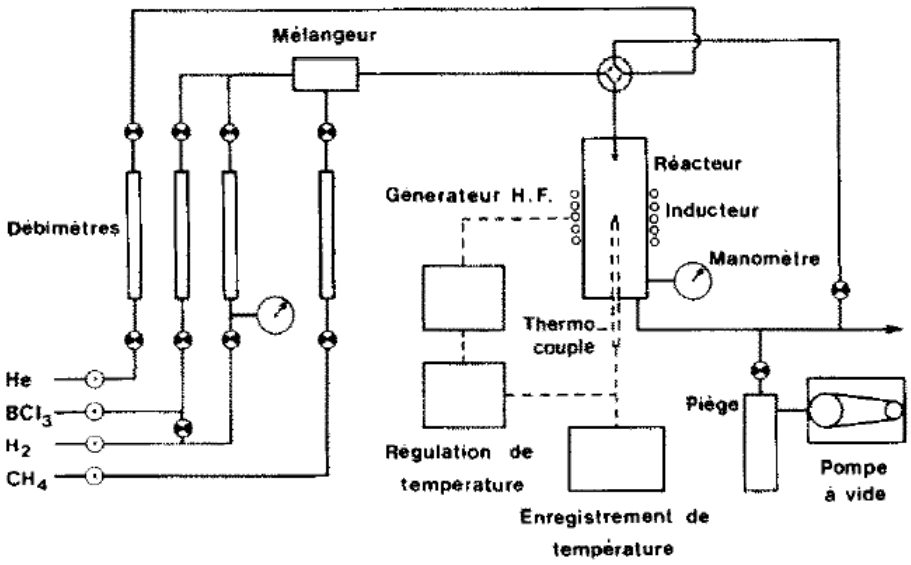

Figure 4: Schematic of Cold Walled CVD System [20]

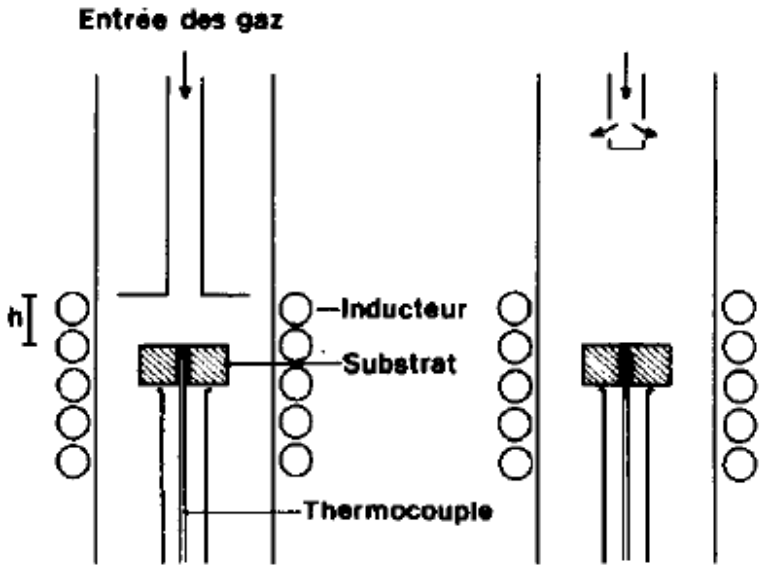

Figure 5: Graphite Substrate Deposition Surface [20]

The boron to carbon ratio in the deposited films was determined to be dependent on the partial pressure of the methane gas and on the temperature of the reactor. The phases in the diagram below are produced under near-equilibrium conditions. However, other phases are often obtained in CVD systems through other kinetically favored, non-equilibrium conditions of deposition. The phase domains of B-C structures can be seen in Figure 6.

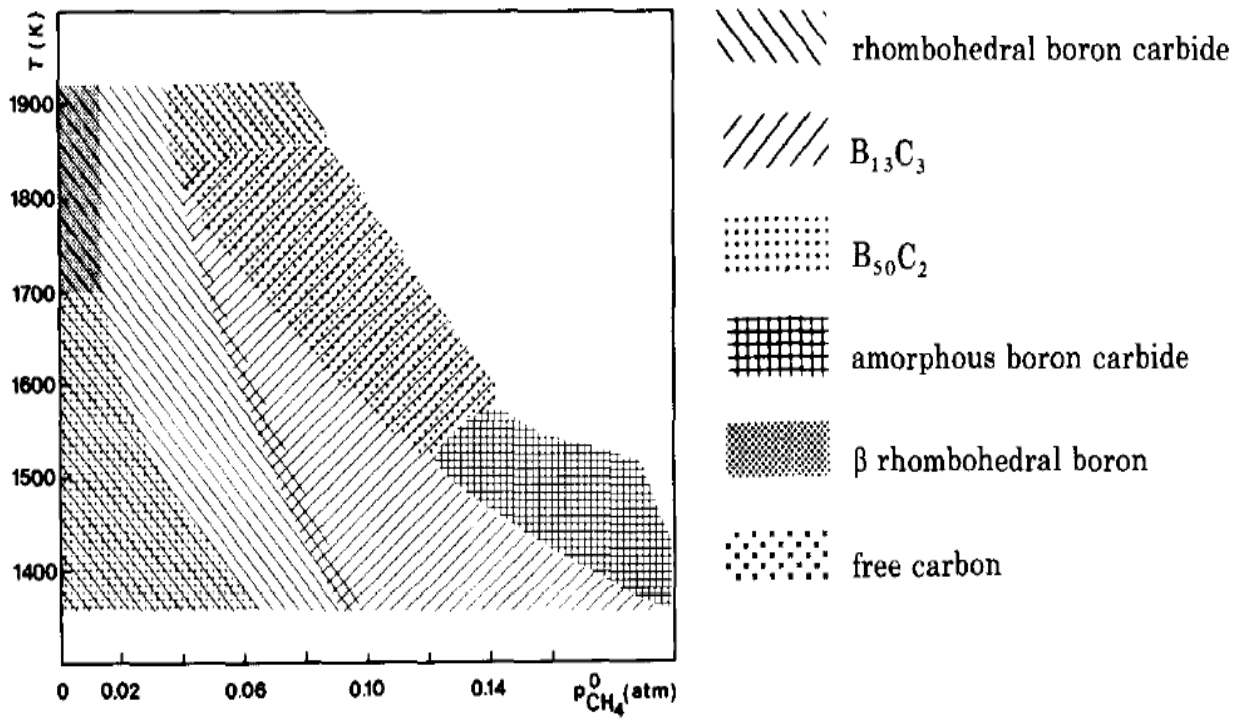

Figure 6: Deposition Domains of the Various Structures as a Function of *T* and the Partial Pressure of Methane [20]

1.3.2 LPCVD of Boron Carbide on Boron

In 1989, Jansson *et al* grew thin films of boron carbide on a 5-10 μm thick layer of α-rhombohedral boron using a BCl_4-CH_4-H_2 thermal decomposition cold walled CVD system [7]. This growth was carried out at a reduced pressure of 1.3-6.7 kPa, a constant H_2:BCl_3 molar ratio of 10, and a temperature range of 1300-1500 K. Many different stable phases of boron carbide were grown, including $B_{13}C_2$, $B_{51}C$, $B_{50}C_2$, and $B_{49}C_3$. Three different experimental parameters were modified to observe the effect on the film growth: the influence of temperature (1300-1500 K), the influence of both methane and boron trichloride vapor composition, and the influence of total pressure (1.3-6.7 kPa). The rhombohedral phase $B_{13}C_2$ was deposited at higher methane concentrations in the vapor. Carbon concentrations in $B_{13}C_2$ ranged from about 7-15 at.%,

compared to the generally accepted homogeneity range of 9-20 at.%. From the pressure parametric study, it was concluded that higher carbon concentrations could be obtained by growing at higher temperatures and lower pressures. This can be seen in Figure 7.

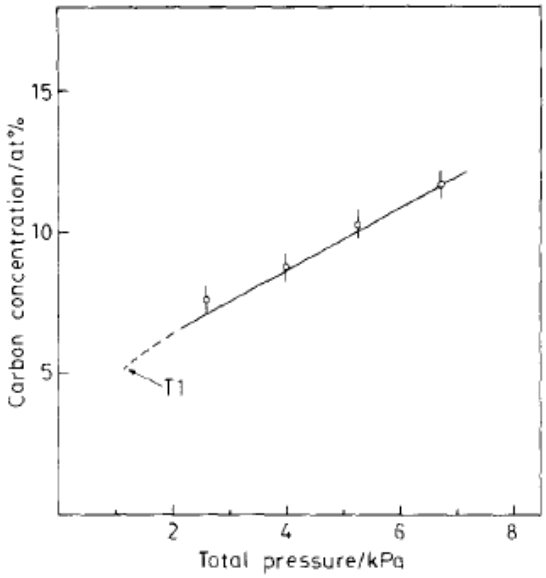

Figure 7: Carbon Concentration as a Function of Total Pressure [7]

Significant discrepancies were observed between experimental deposition and calculated deposition diagrams. The calculations predicted that rhombohedral boron carbide would be formed for small methane concentrations in the vapor and also predicted that nearly all of the methane would react to form boron carbide or free carbon in the form of graphite. However, rhombohedral boron carbide proved to be quite difficult to grow, and carbon content in the films was low even at high methane concentrations. The major reason for this was concluded to be a kinetic nucleation barrier that inhibits the deposition of carbon. Overall, comparisons of

experimental results to the thermodynamic calculations proved that the deposition of boron carbide via CVD occurs far from equilibrium conditions.

1.3.3 LPCVD of Boron Carbide on Graphite

In 2009, Liu *et al* grew boron carbide thin films up to 18.0 µm thick onto 30mm x 15mm x 2mm graphite wafers using LPCVD. The deposition occurred in a vertical, hot wall furnace with a 200 mm inner diameter at a fixed pressure of 10 kPa. This system used the BCl_4-CH_4-H_2 thermal decomposition mechanism to deposit the boron carbide thin film. Several parametric studies on boron carbide deposition rate were conducted by this group, including the effect of deposition time and temperature, the effect of inlet BCl_3/CH_4 gas ratio, and the effect of inlet H_2/CH_4 gas ratio. The experimental apparatus can be seen in Figure 8.

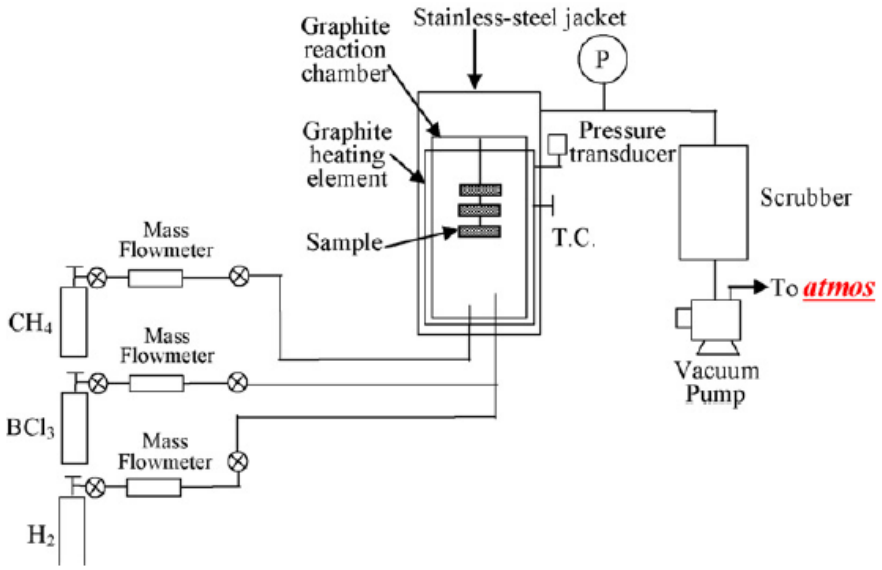

Figure 8: Schematic of the Vertical Hot-Wall Reactor used to Deposit Boron Carbide [8]

Regression analysis for both relative weight gain rate and thickening rate as a function of the deposition parameters was done using Uniform Design software. From the parametric studies, it was determined that the deposition rate varies exponentially with the temperature. The deposition rate varies linearly with the deposition time and the inlet BCl_3/CH_4 gas ratio, also called δ. The results from the parametric studies can be seen in Figures 9 and 10.

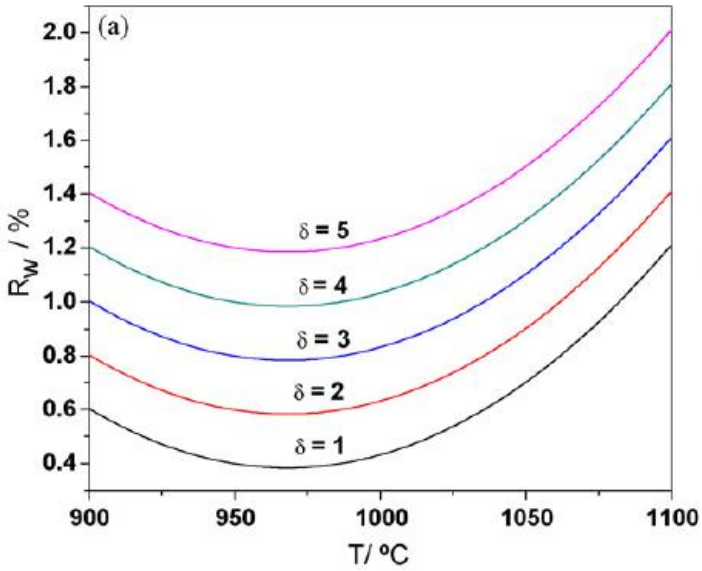

Figure 9: Relation Curve between Relative Weight Gain and Deposition Temperature at five inlet BCl_3/CH_4 gas ratios [8]

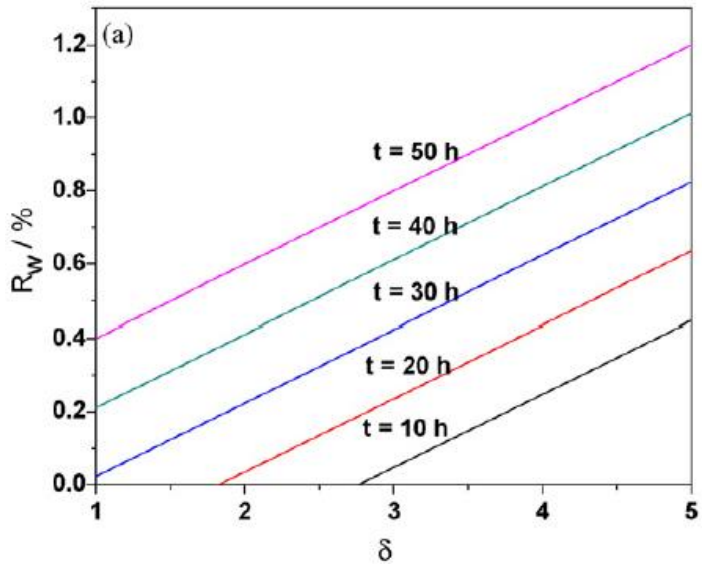

Figure 10: Relation Curve between Relative Weight Gain and Inlet BCl_3/CH_4 Gas Ratios at 5 different deposition times [8]

Of the deposition parameters studied, it was determined that the deposition temperature had the greatest effect on the microstructure of the deposited boron carbide film. At high temperatures (1050-1100°C), the deposited films were constituted by two interlaced phases, PyC and B_4C. Both of which had low boron concentrations ranging from 40-49 at.%. At low temperatures (900-950°C), layered and dense B_4C with high boron content of approximately 79 at.% was grown. The optimized deposition parameters, according to highest growth rate, were reported to be T=1100°C and δ=5.0 with an inlet H_2/CH_4 gas ratio of 3.5 and a deposition time of 50 hours [8].

Chapter 2: Experimental Methods

2.1 Reactant Gas Selection

Boron carbide thin films have been grown in non-plasma CVD systems using several different reactant gas combinations, including BCl_3-CH_4-H_2 and BCl_3-CCl_4-H_2. In addition, boron carbide films have also been grown via Plasma Enhanced Chemical Vapor Deposition (PECVD) using a B_2H_6-CH_4-H_2 gas mixture [21]. Within each experiment, the stoichiometry and properties of the deposited films varied with deposition parameters, such as temperature, pressure, and reactant gas ratios. However, it was demonstrated that B_4C could be grown using both the BCl_3-CH_4-H_2 and the BCl_3-CCl_4-H_2 system. Thus, the safety of the possible reactant gases was considered. Boron trichloride, BCl_3, is described as a colorless, very corrosive, and highly toxic gas. Diborane, B_2H_6, is described as a highly toxic gas that forms explosive mixtures and ignites spontaneously in air. Methane, CH_4, is a colorless and flammable gas. Carbon tetrachloride, CCl_4, is described as a colorless and toxic gas. Due to the lower risk that BCl_3 poses to personnel as opposed to B_2H_6, BCl_3 was chosen as the boron-containing reactant gas. While CH_4 is flammable, it is non-toxic. Since CCl_4 is a toxic gas, it is more dangerous to humans than CH_4. So methane was chosen as the carbon-containing reactant gas. At 900°C, boron carbide is deposited via the reaction products nucleation mechanism, which is shown in Figure 11.

$$2CH_4 \rightarrow s{\cdot}C_2H_2 + 3H_2$$

$$BCl_3 + H_2 \rightarrow s{\cdot}HBCl_2 + HCl$$

$$s{\cdot}HBCl_2 + s{\cdot}C_2H_2 \rightarrow s{\cdot}B_4C + HCl$$

Figure 11: Boron Carbide Reaction Products Nucleation Mechanism [8]

2.2 Design of Low Pressure CVD System

The low pressure CVD system developed for this project is comprised of three high purity gas tanks compression fitted to ¼" outer diameter 316 stainless steel tubing to a high purity quartz processing tube in a GSL-1500X-50 high temperature tube furnace purchased from MTI Corporation. On either side of the heating zone inside the furnace, the processing tube is thermally insulated with alumina foam cylinders 40 mm in diameter and 60 mm in length. Mass flow rates and the corresponding boron to carbon molar ratio of the reactant gases were controlled with Parker Model 201 fast-response analog mass flow controllers (MFCs); these MFCs were fitted with Kalrez elastomer seals, due to the outstanding chemical corrosion resistance of Kalrez.

The furnace was evacuated using a chemical-resistant and Teflon-coated Welch 1402 vacuum roughing pump. The growth substrate for the boron carbide thin films was the (100) plane of the polished side of phosphorus doped n-type silicon wafers with resistivity of 1-10 Ohm-cm purchased from Silicon Inc. The surfaces of the wafers were held parallel to the flow of the gases by a quartz boat 101 millimeters in length. The quartz boat was placed in the center of

a 30 inch long quartz tube with 46 millimeters inner diameter. A picture of the seven silicon wafers on the quartz boat before entering the tube furnace is shown is Figure 12.

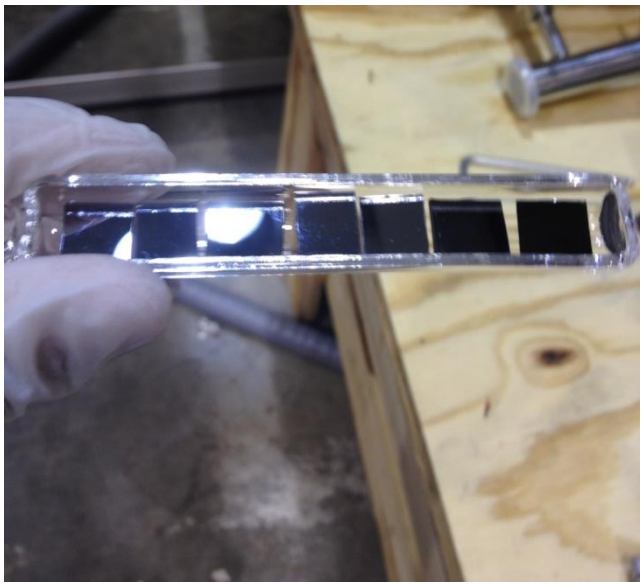

Figure 12: Picture of Seven Silicon Wafers in Quartz Boat

Concerning the placement of the wafers within the quartz growth tube, the quartz boat was placed at the center of the 30 inch long quartz tube. A diagram of the 1 square centimeter silicon wafer orientation is shown in Figure 13 with the seven silicon wafers pictured in red.

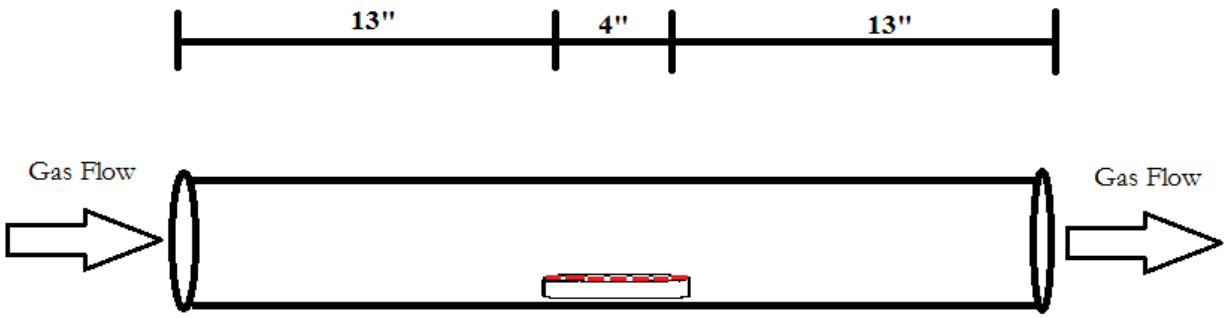

Figure 13: Diagram of Silicon Wafer Placement

A Welch 1420H-14 liquid nitrogen cold trap was used to prevent vacuum pump oil from backstreaming into the growth chamber. Macurco HD-11 hydrogen gas detectors were placed above the MFCs mounted on the wall and above the tube furnace. The gas detectors were then wired in series to three Asco 8262H186V normally-closed solenoid valves, which were placed in each of the gas lines as close to the each of the three gas tanks as reasonably possible. This way, in the case of a leak in the system or a complete power outage, the solenoid valves would close and impede uncontrolled gas release. A schematic of the CVD system is shown in Figure 14.

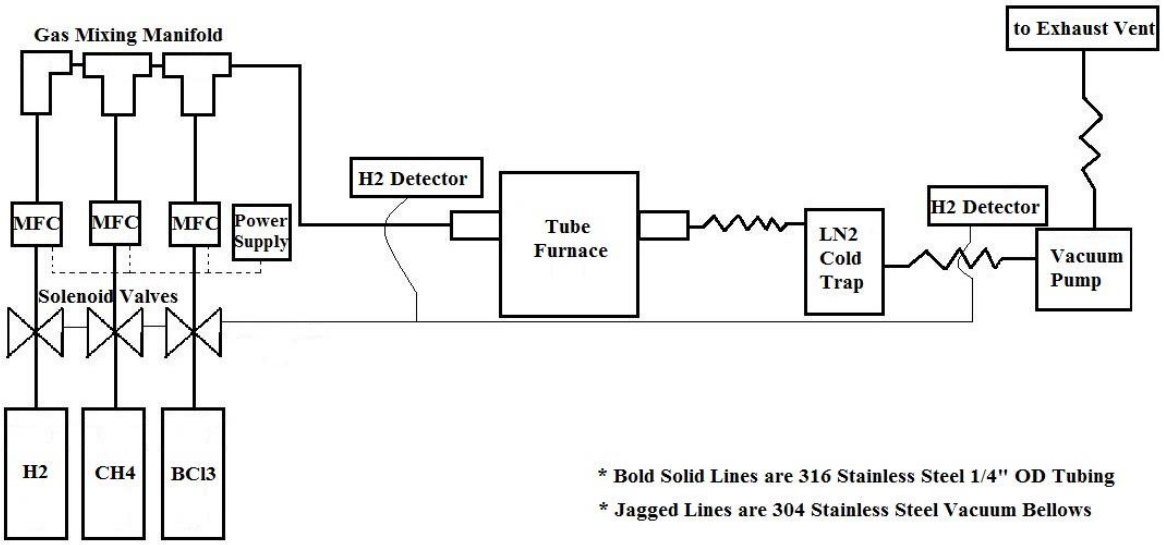

Figure 14: Hot Walled CVD Schematic

2.3 Methodology

In order to conduct the boron carbide growth, the tube furnace containing the quartz boat and the seven one square centimeter silicon wafers was evacuated to 5 milliTorr and then heated to approximately 900°C at a rate of 15°C per minute. Ultra High Purity (99.9995% H_2) hydrogen gas was introduced into the system at 350 standard cubic centimeters per minute (sccm). Chemically Pure (99.9% BCl_3) boron trichloride and Ultra High Purity (99.99% CH_4) methane were then introduced into the system at a ratio of 5:1 at 500 sccm and 100 sccm, respectively. The flow of the gases caused the system pressure to increase, which stabilized during the growth at 25 Torr. The work of Liu *et al* demonstrated that amorphous boron carbide could be grown at a rate of 0.09 µm/hour using very similar parameters [8]. The growth was conducted for three hours, at which point the reactant gases were turned off at the tank regulators. Hydrogen gas was left flowing at 350 sccm for five minutes to purge any residual reactant gases. The system was

then cooled down to room temperature at a rate of 15°C per minute. Once cool, the CVD system was vented to atmospheric pressure, the quartz boat was withdrawn from the furnace, and the samples were carefully removed from the boat using tweezers. A picture of the quartz boat after the growth is shown in Figure 15.

Figure 15: Quartz Boat Post Boron Carbide Growth

Chapter 3: Results and Discussion

3.1 Thin Film Surface Characterization

The boron carbide thin films deposited onto the silicon wafers appeared to be mostly uniform across the seven wafers, with some wafers containing a small amount of bare, polished silicon surface area without the black boron carbide. The surface features were viewed with a Zeiss Auriga Dual Beam FIB/SEM and a Zeiss Libra 200 Field Emission Monochromator TEM.

For one of the seven samples, the elemental composition of the deposited film was analyzed using laser induced breakdown spectroscopy (LIBS). This was accomplished using an Ocean Optics LIBS system with 0.055 nm spectral resolution and ADDLibs spectral analysis software. Laser induced breakdown spectroscopy is a form of atomic emission spectroscopy that involves ablating the surface of the material with a focused, low power laser. The surface material is heated such that it is vaporized into plasma; as elemental ions composing the plasma de-excite, they emit photons of characteristic energy and wavelength [22]. Over the last few decades, LIBS has become an increasingly popular method for elemental analysis of semiconducting thin films, including impurity identification, qualitative and quantitative determination of doping concentrations, and elemental depth profiling [23].

3.1.1 SEM Micrographs

Inspecting the samples using the SEM, the surface of the sample could be seen to have fairly uniform deposition of a pebble-like coating, as well as non-uniform deposition of various sized whisker clusters. In Figure 16, a SEM micrograph of the surface of a boron carbide-silicon

wafer is shown. One can distinguish areas (in the top left quadrant of the picture) where the boron carbide did not deposit onto the silicon wafer. Also, nanowhisker cluster structures can be seen on the surface of the deposited film.

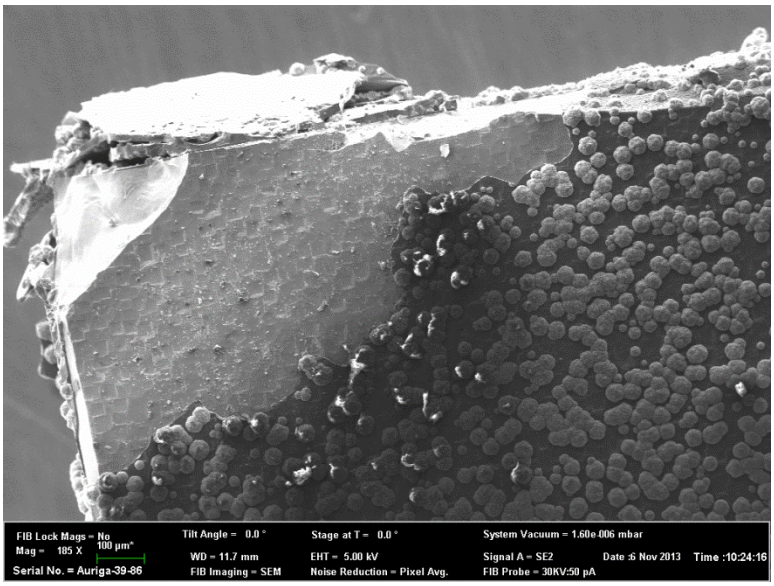

Figure 16: SEM Micrograph of the Boron Carbide-Silicon Surface

The clusters were measured to be an average of 25 microns in diameter and were determined to be composed of nanowhiskers of diameters varying from 150-200 nm, suggesting a preferential growth mechanism in the vertical direction [24]. In Figure 17, a close-up shot of the round clusters can be seen.

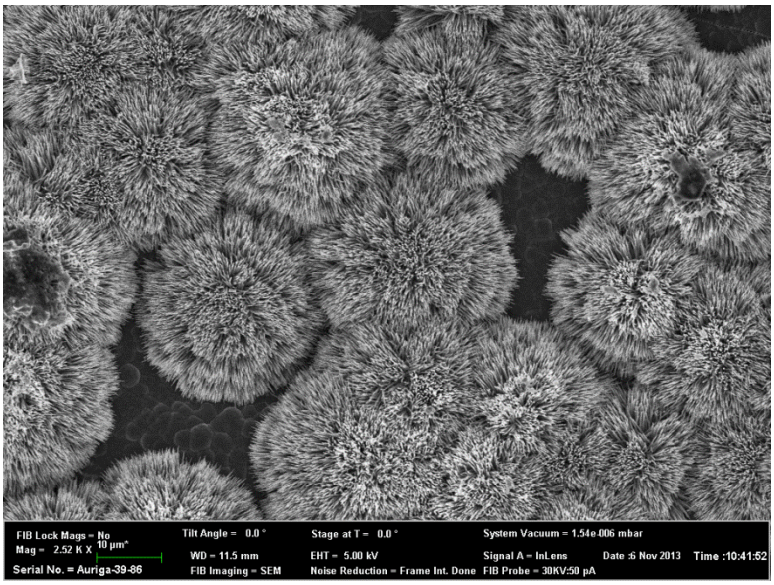

Figure 17: Nanowhisker Round Clusters

3.1.2 TEM Micrographs

The boron carbide-silicon wafer that had the most even boron carbide deposition was scraped using a razor blade to obtain small flakes of the deposited material. Very thin flakes of material (thickness of <100nm) are needed for proper TEM characterization, due to significant electron energy loss in thicker samples. The scraped flakes were then sonicated in methanol for twenty minutes to break the flakes into the smallest possible pieces. A pipette was used to transfer the methanol-boron carbide flake solution onto a carbon grid TEM slide on top of filter paper, which was then dried for ten minutes at 150°C.

In Figure 18, a small shard of the boron carbide pebble-structure thin film can be seen sitting on top of a lacey carbon sample holder. The objects that appear to be holes are vacuum or empty space. It can also been seen that multiple shards are stacked on top of each other, skewing the TEM image.

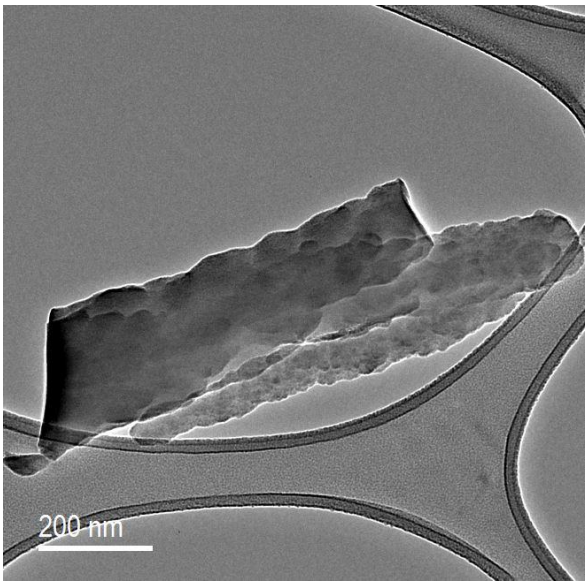

Figure 18: TEM Micrograph of Boron Carbide Shard

In Figure 19, the interface between the boron carbide shard and the vacuum region can be seen. The vacuum region is in the top left quadrant of the picture. The majority of the picture is the surface of the boron carbide shard. One can see the growth direction of crystallographic planes in an array, indicated by the white arrows. The surface also exhibits random texturing, meaning that there is variation in the growth direction of the boron carbide crystallites. This suggests that the crystallography of the shard is polycrystalline.

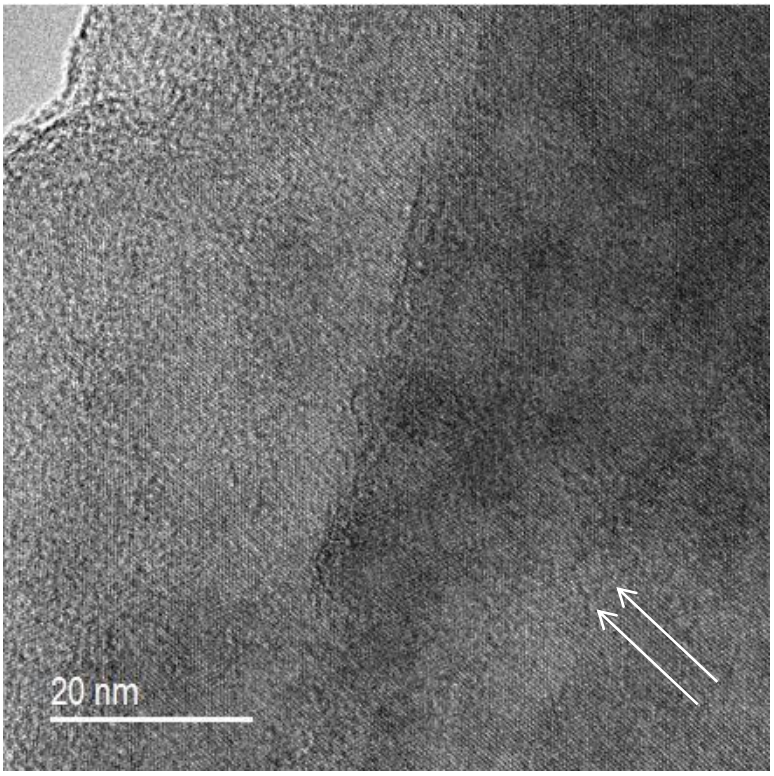

Figure 19: TEM Micrograph of Vacuum-Shard Interface

In Figure 20, the Fast Fourier Transform (FFT) of the electron diffraction pattern through the material can be seen. There are a few diffractions from crystallographic planes. However, the diffraction spots are inconsistent, indicating that the material scraped from the film lacks a homogenous, single crystalline structure. In addition, concentric circles, which indicate the presence of an amorphous material, can be seen in the FFT [25]. Thus, the shards have polycrystalline structure with some amorphous regions.

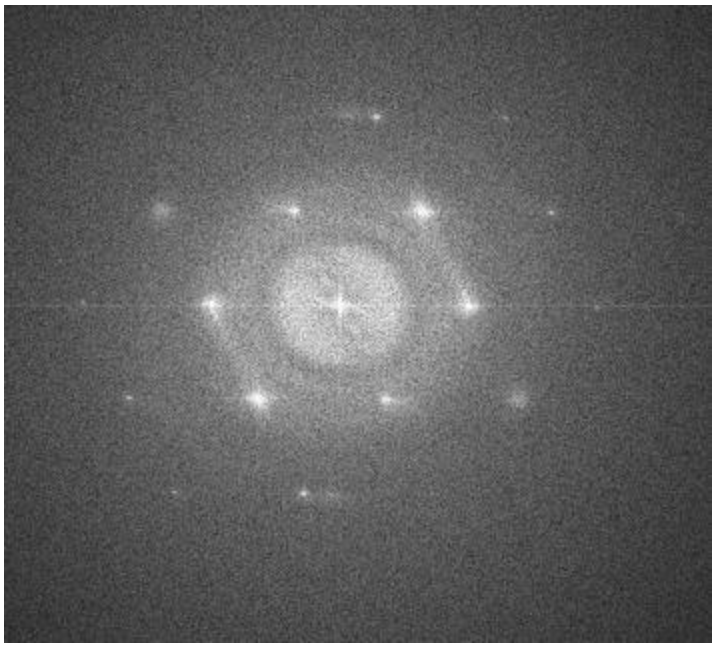

Figure 20: FFT Diffraction Pattern of Vacuum-Shard Interface

Electron diffraction studies and energy dispersive x-ray spectroscopy were to be performed on the grown nanowhisker structures. However, due to the size of the whiskers, they could not be isolated onto a TEM slide without other structures becoming stacked and interfering with the signal generated through the electron diffractions. For this reason, the elemental composition and crystallography of the nanowhiskers remains to be determined.

3.1.3 LIBS Analysis

Several different techniques of laser ablation were used, including grid spot ablation, low and high power laser settings, ablation depth profiling, and adding a gate delay to the spectrometer to account for the time it takes for the plasma to de-excite. Spectral data was taken using the Ocean Optics LIBS system, which was then analyzed both with the ADDLibs software

and Microsoft Excel 2010. Only one of the seven grown samples was analyzed with LIBS, due to time constraints associated with use of the LIBS system at Y-12 National Security Complex. The spectroscopic accuracy of the laser was tested by using a CVD diamond as a calibration material. The CVD diamond was purchased through Element 6. The CVD diamond calibration spectrum is shown in Figure 21.

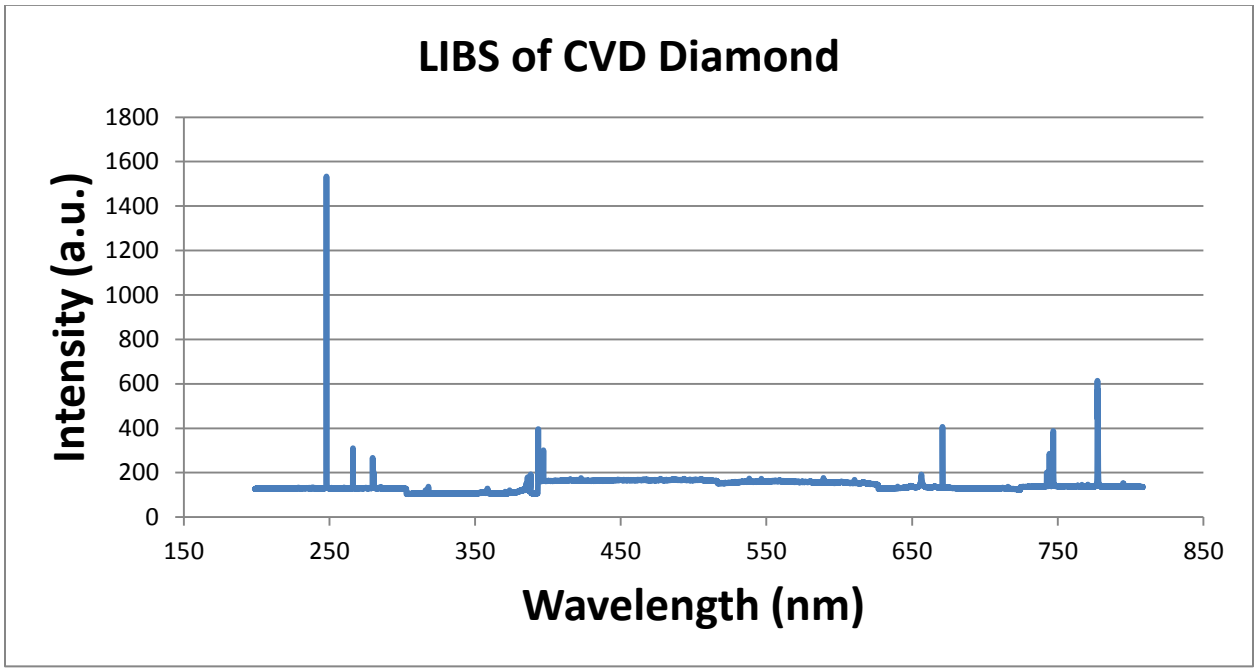

Figure 21: CVD Diamond Calibration Spectrum

Comparing this data to the known NIST database of elemental spectral lines, the CVD diamond calibration spectrum is very accurate [26]. The primary carbon spectral line at 247.8 nm can be clearly seen, indicating that the LIBS system is properly calibrated for detecting carbon.

After the CVD diamond calibration test, the boron carbide surface was ablated by the laser to analyze the elemental content of the deposited film. A picture of the boron carbide

surface before ablation, with a scale bar of 100 µm in the upper left corner, can be seen in Figure 22.

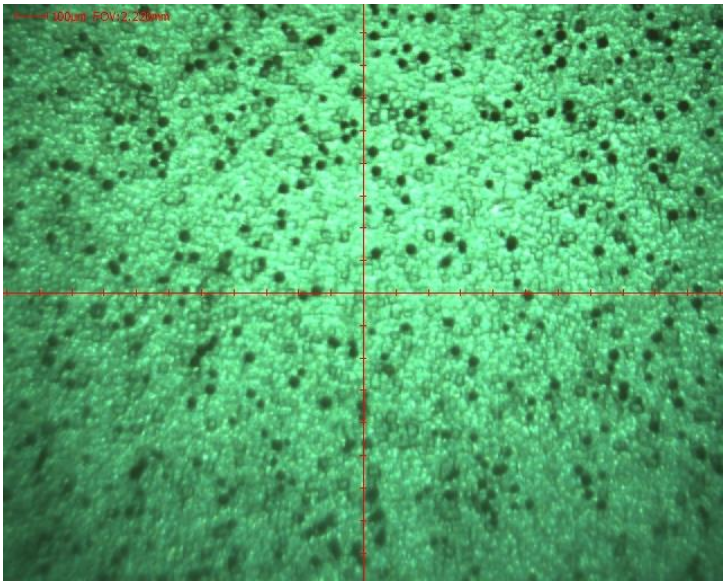

Figure 22: LIBS Optical Microscope Picture of Boron Carbide Surface Pre-Ablation

In Figure 23, a picture with the same 100 µm scale as Figure 9 shows the boron carbide surface after 1 shot at 100% power with a 1 microsecond gate delay on the LIBS spectrometer.

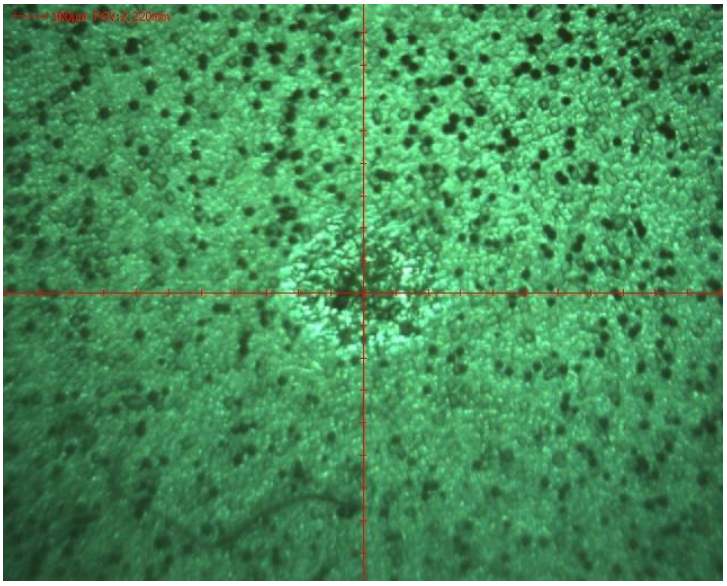

Figure 23: LIBS Optical Microscope Picture of Boron Carbide Surface Post-Ablation

A high resolution, real color picture can be seen of the single shot ablation in Figure 24. This picture was taken using a Keyence Optical/Laser Profilimeter. One can see where the boron carbide was ablated from the surface of the wafer. In addition, one can also clearly see the unpolished silicon wafer underneath the deposition.

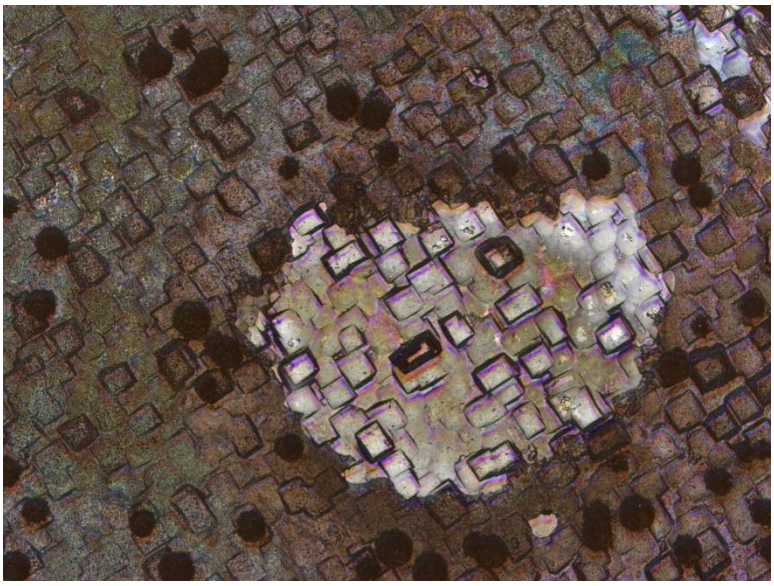

Figure 24: Real Color Picture of Surface after 1 shot at 100% Laser Power

It was determined after this ablation that the boron carbide material would be able to withstand blasts from the laser at 100% power. If the laser had blown straight through both the boron carbide and the silicon, then the power would need to be decreased. Next, a 7x7 grid of 300 micron diameter spots spaced 400 microns apart was ablated at 100% laser power with a 1 microsecond gate delay. This grid was blasted three separate times in order to create an elemental depth profile as the laser bore deeper into the surface of the wafer. A picture of the boron carbide surface post-grid ablation can be seen in Figure 25.

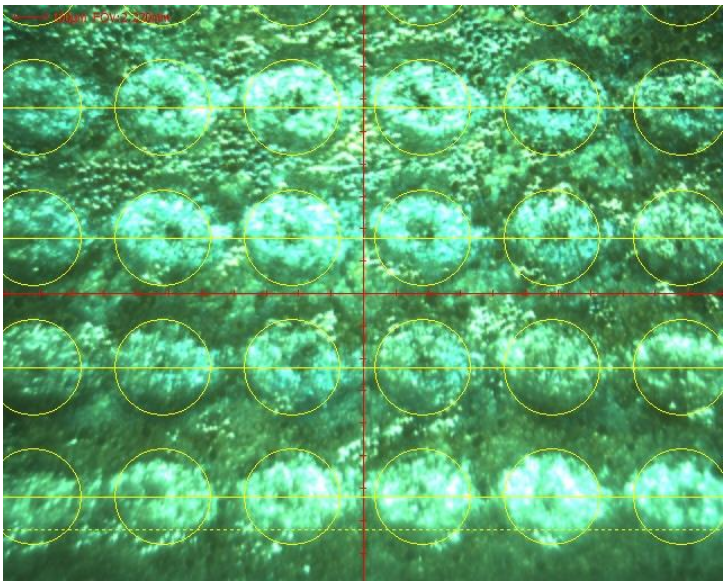

Figure 25: Boron Carbide Surface Area after 2 Grid Shots at 100% Laser Power

The spectrum of the three ablation scans can be seen in Figure 26. The boron spectral line at 249.3 nm and the carbon spectral line at 247.8 nm are both difficult to see in the full range of the spectrum from 200-800 nm. However, the peaks from the spectral lines are clearly seen in the spectral range of 247-254 nm. In Figure 27, the spectrum from 247-254 nm is examined.

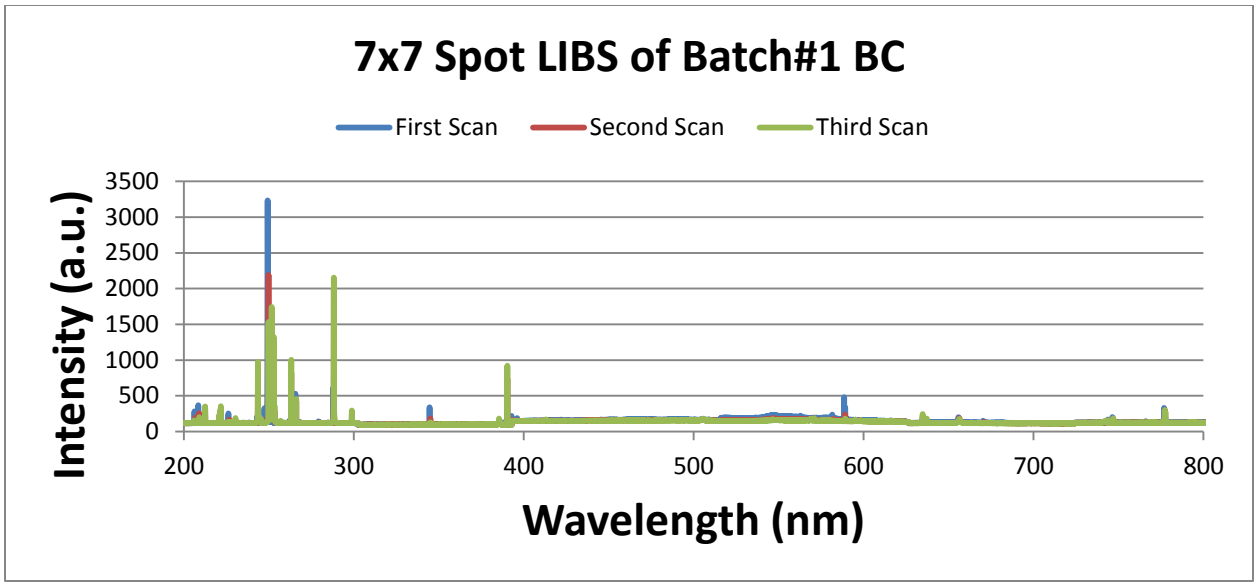

Figure 26: 7x7 Grid Spot LIBS at 100% Laser Power and 1 Microsecond Gate Delay

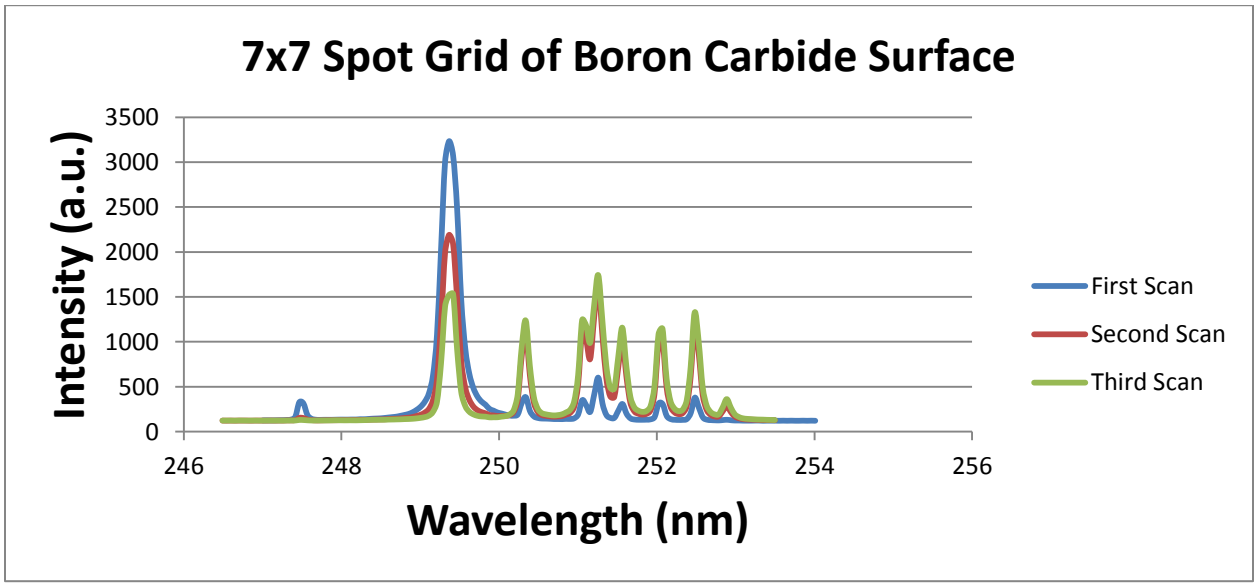

Figure 27: 7x7 Grid Spot LIBS 246-256 nm

The results indicate that the surface has a thin layer of boron carbide deposition on top of the silicon wafer. Boron spectral lines are seen at 249.3 nm, 344.7 nm, and 588.6 nm. These lines

are much more intense for the first scan of the surface. Then, as the laser bores deeper into the material, it passes through the boron carbide layer and into the silicon substrate. Silicon spectral lines at 243.6 nm, 251-252 nm, 288.3 nm and 390.6 nm are more prominent on the third scan [26]. This suggests that the boron carbide layer was bored through, and the silicon substrate was breached by the laser.

One can take the ratio of the sum of the counts under the boron and carbon spectral peaks in order to qualitatively estimate the ratio of boron to carbon in the films. When doing this, the emission intensity of the spectral lines was taken into account. For the 7x7 grid spot that was analyzed, which is about a 3.1 mm by 3.1 mm square area of the one square centimeter wafer, the boron to carbon ratio was estimated to be around 2:1. This suggests that boron atoms were more readily absorbed into the boron carbide films than carbon atoms, disagreeing with the findings of Liu *et al* that carbon concentrations are higher when boron carbide is grown at temperatures higher than 900°C [8].

After obtaining data with the LIBS system, the laser was used to blast deep into the surface of the wafer. This was done by selecting a 300 micron diameter spot and ablating with 100% laser power twenty times in a row. The laser appeared to have a melting effect on the boron carbide surface and silicon substrate, as melted ripples can be seen leading to the ablation hole. A real color picture of the twenty shot laser ablation hole in the boron carbide surface can be seen in Figure 28.

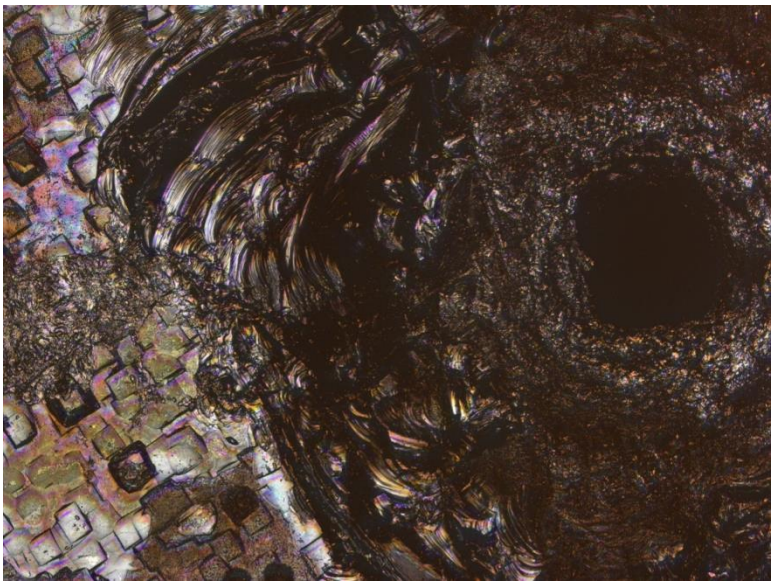

Figure 28: Twenty Shot Laser Ablation Hole on Surface of Boron Carbide

3.2 Boron Carbide-Silicon Interface Characterization

The interface between the silicon substrate and the deposited films was characterized using a Zeiss Auriga SEM equipped with gallium Focused Ion Beam (FIB) milling and platinum microlayer deposition capability and a Zeiss Libra 200 Field Emission Monochromator TEM equipped with electron energy loss spectroscopy (EELS) with an energy resolution of 0.2 eV. The FIB milling capability of the SEM was utilized primarily for preparing thin (<1 micron) samples of the boron carbide-silicon interface. The TEM used is capable of imaging defects and impurities within the crystalline material, due to its spatial resolution of 0.24 nm. In addition, the high resolution transmission electron microscopy (HRTEM) capabilities of this microscope can provide the researcher with useful information about crystallography, grain boundaries, and crystal phases of a given sample. The interface was examined in the TEM in order to analyze the epitaxy between the film and substrate, as well as to perform electron diffraction studies of the deposited films.

3.2.1 SEM Preparation

In order to create a proper sample for TEM and EELS analysis, a very thin sliver, called a lamella, of the boron carbide and silicon interface is sliced out of the sample. This is done by milling into the surface of the wafer using a FIB of gallium ions. An SEM micrograph of the surface of the sample before lamella extraction is shown in Figure 29.

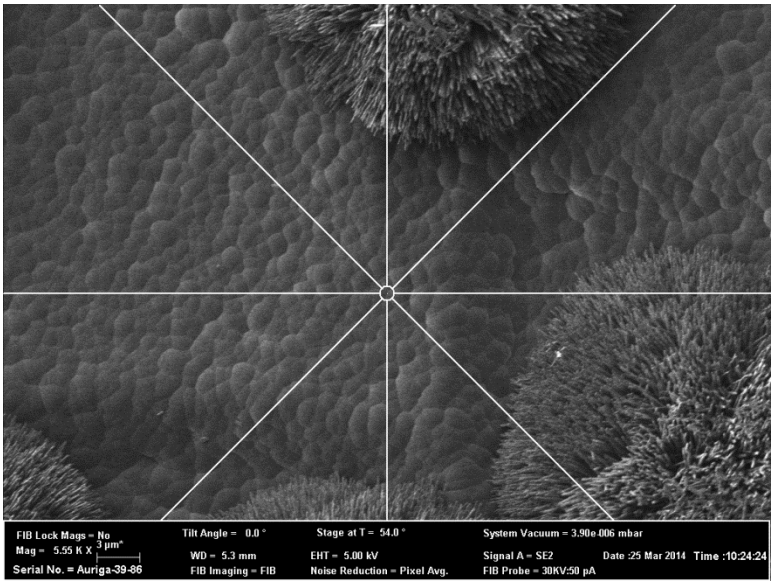

Figure 29: SEM Micrograph of Boron Carbide Surface

A 2 micron by 15 micron protective platinum strip is deposited where the lamella is to be extracted. The platinum strip on the surface of the wafer can be seen in Figure 30.

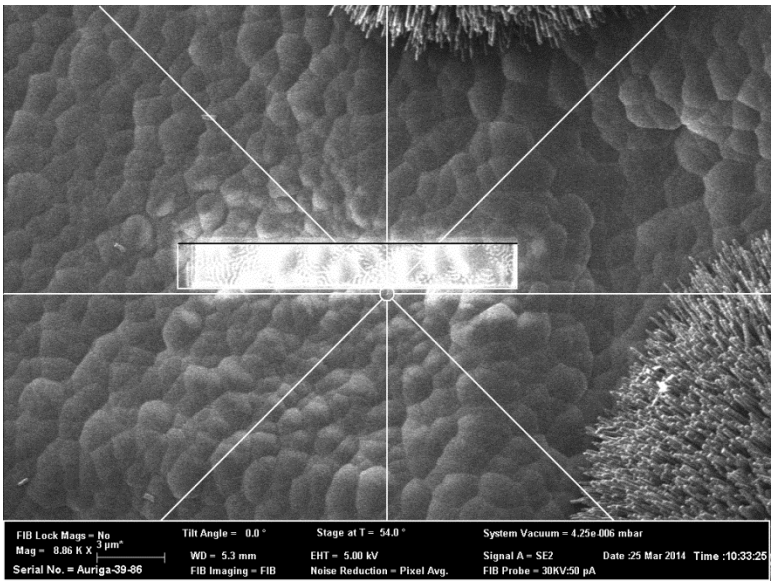

Figure 30: SEM Micrograph of Protective Platinum Strip

Trapezoidal areas on three sides of the platinum strip are then milled about 10 microns into the surface of the wafer at a 20 degree angle to the surface. The sides of the lamella are then FIB polished so that the thickness of the sliver is about 500 nanometers. A polished lamella topped with a platinum strip that is ready for extraction is shown in Figure 31.

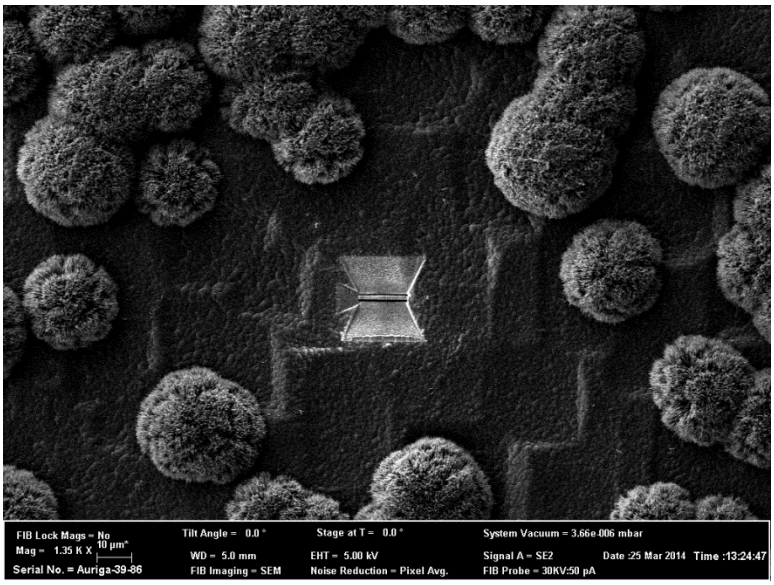

Figure 31: Lamella in Milled Trench on the Boron Carbide Surface

A magnified image of the lamella inside the milled trench is shown in Figure 32.

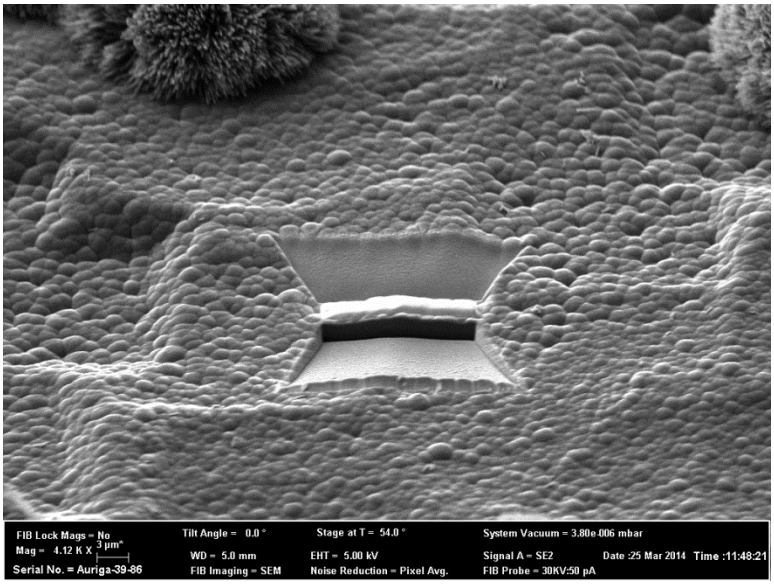

Figure 32: Magnified SEM Micrograph of Lamella Inside Milled Trench

The lamella is then welded to a tungsten needle using platinum and detached from the sample using the FIB in order to attach the lamella to the post of a copper grid used for TEM analysis. Once the lamella was attached to the copper grid, three sections of the lamella were FIB milled to a thickness of about 100 nm. Milling to this thickness allows the electrons in the TEM to pass through the material for electron diffraction and energy loss studies.

3.2.2 TEM Analysis

Once the copper grid containing the lamella is loaded into the TEM, the lamella was found on the screen and examined. The three sections that were thinned by the SEM, indicated by red arrows, are more transparent than the thicker sections. The platinum weld can be seen where the lamella connects to the grid post. In addition, the platinum protective layer is seen atop the lamella in the sections that have not been thinned to 100 nm. The lamella welded atop the copper grid post is shown in Figure 33.

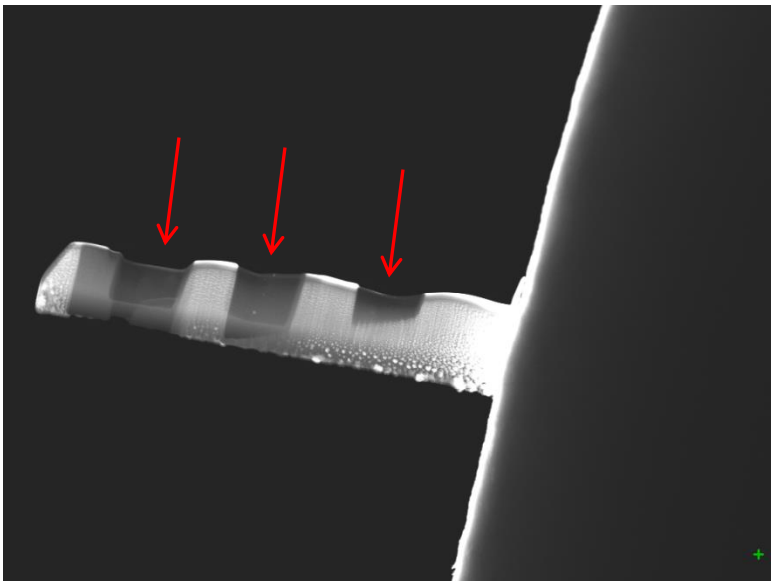

Figure 33: Lamella Welded to the Copper Grid Post

The section furthest from the copper grid post was magnified and focused on. The silicon substrate is seen at the top of the picture. This is followed by a layer of boron carbide approximately 200 nm in thickness. The final layer seen at the bottom of the screen is the platinum. The boron carbide-silicon interface within this section can be seen in Figure 34.

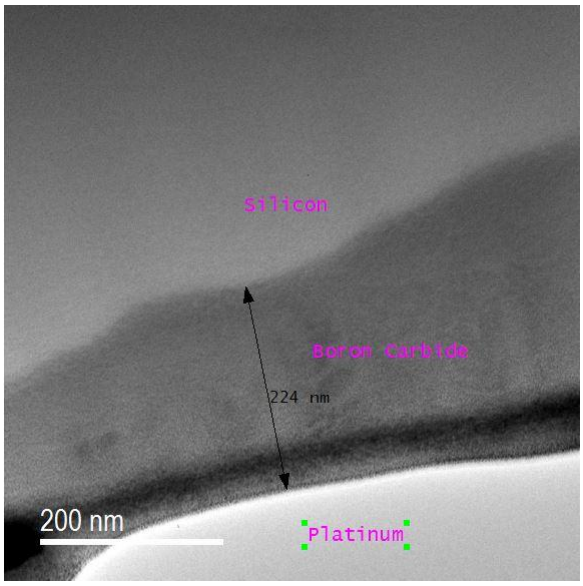

Figure 34: TEM Micrograph of Boron Carbide-Silicon Interface

The thinned sections were then analyzed using electron diffraction studies at different areas in order to determine the crystalline structure of the boron carbide composing the lamella. The diffraction pattern from the thinnest section of boron carbide on the lamella is shown in Figure 35. Once again, concentric diffraction rings can be seen. This time, however, no coherent plane diffraction lines can be seen, indicating that the thinnest section of boron carbide on the lamella is strictly amorphous.

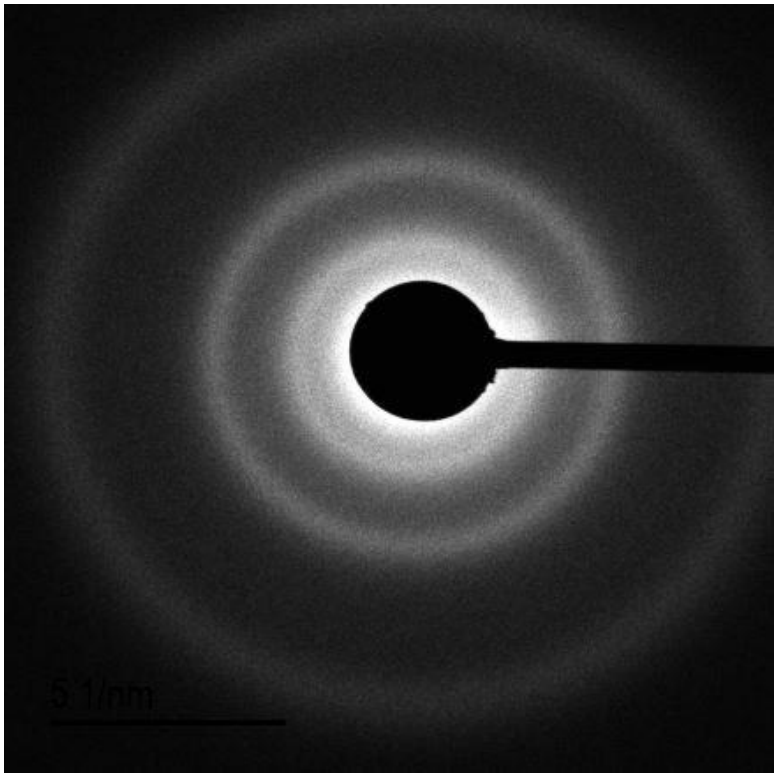

Figure 35: FFT of Thinnest Boron Carbide Section on Lamella

The next thinnest section was then analyzed at various magnifications in order to determine the crystallinity of the boron carbide within that section. TEM micrographs of the thinned boron carbide section at various magnifications and the corresponding FFTs of the electron diffraction patterns can be seen in Figure 36. The interface between the lamella and the vacuum region (empty space) is seen at the bottom of the micrographs. Within the actual TEM micrographs, no coherent crystal plane lines can be seen. The entire surface of the material is of granular and non-oriented structure. Even the TEM micrograph of the boron carbide surface at high magnification indicates no presence of arrayed crystal planes. Concentric diffraction rings can be seen at each magnification. Furthermore, no diffraction spots or lines indicative of crystallographic planes are present in any of the FFTs. This is conclusive evidence that the boron

carbide within the lamella is amorphous. Due to the lack of boron carbide single crystallinity at the substrate-film interface, epitaxy was not achieved between the boron carbide thin film and the silicon substrate. It is hypothesized that the amorphous pebble-like layer.

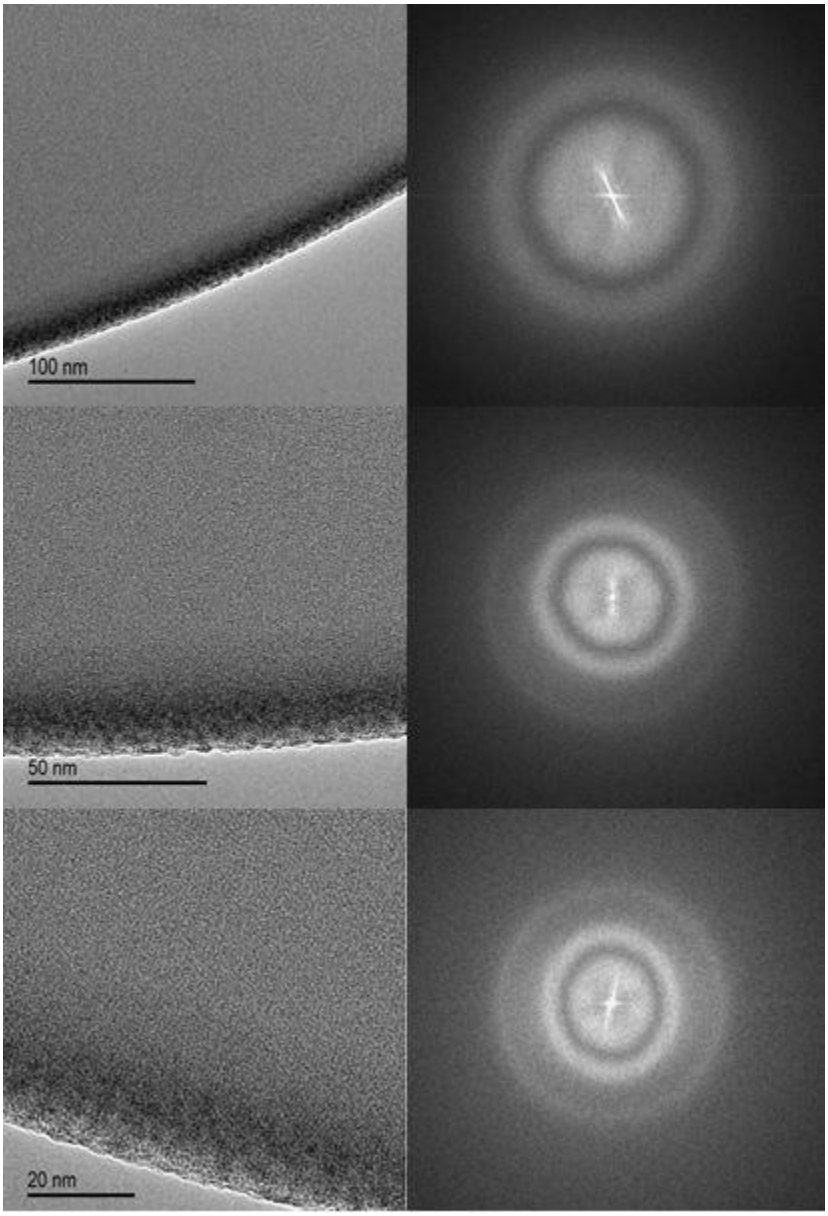

Figure 36: TEM Micrographs and Corresponding FFTs of Boron Carbide within Lamella

The boron carbide thin film layer was then was analyzed using Energy Dispersive X-Ray Spectroscopy (EDS). When electrons interact with materials and lose energy, x-rays are emitted. The energies of the x-rays are characteristic of the element through which the electrons just passed. Thus, EDS can provide both qualitative and quantitative analyses of elemental compositions of materials when characteristic x-rays of significant intensity are detected. An x-ray photopeak is considered significant, when the x-ray count rate is three times that of the background count rate [27]. The spots that were analyzed using the EDS can be seen as white contamination spots in Figure 37.

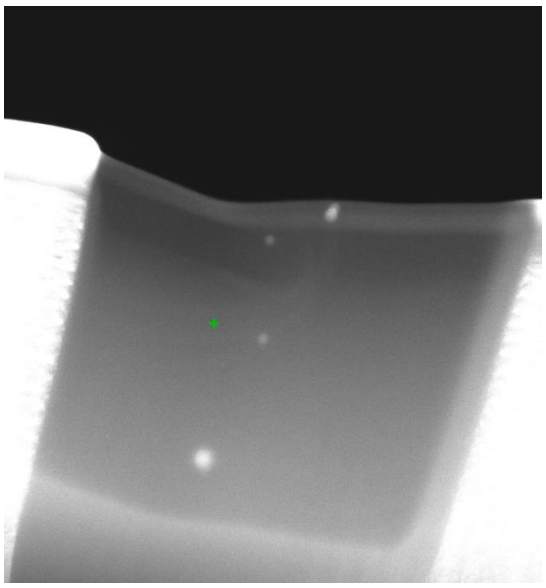

Figure 37: EDS White Contamination Spots

The EDS x-ray spectra indicated that boron and carbon were the primary elements composing the films. The EDS x-ray spectrum can be seen in Figure 38.

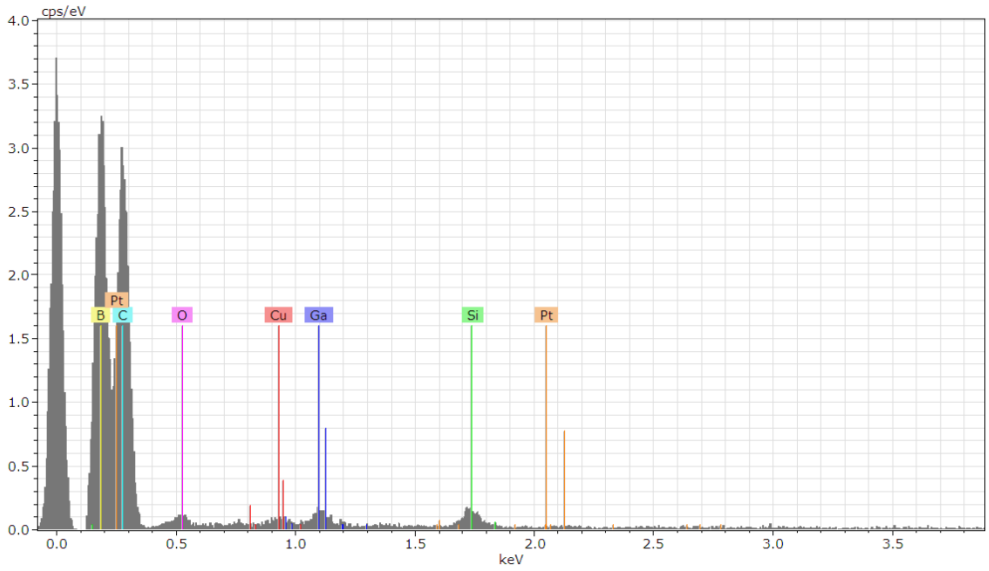

Figure 38: EDS X-Ray Spectrum of Boron Carbide Film

The boron K-edge x-ray can be seen at 188 eV, while the carbon k-edge x-ray can be seen at 282 eV. The copper L-edge x-ray signature at 965 eV is barely above background and is likely from the copper grid post. A small amount of oxygen was detected, as indicated by a miniscule K-edge x-ray peak at 533 eV. This oxygen was probably introduced into the films as an impurity; the source of this oxygen impurity could be from the reactant or carrier gas source, the alumina oxide insulating foam cylinders, chlorine etching of the SiO_2 quartz growth tube could have introduced oxygen radicals into the system, residual moisture from the humid Tennessee air within the stainless steel tubing could have been carried into the growth tube by gases, or many other sources. A small gallium L-edge x-ray peak at 1.134 keV can be seen from the gallium ions implanted into the surface of the lamella from FIB milling. Finally, a small silicon signature can be seen with a K-edge to L-edge transition x-ray peak at 1.740 keV [27]. The source of this silicon peak is from the silicon substrate underneath the boron carbide.

3.3 Electrical Characteristics

Since an ideal p-n heterojunction resists the flow of current in one bias direction, a device composed of p-type boron carbide grown on top of n-type silicon would ideally exhibit the same Schottky diode behavior. This was tested by taking one of the seven wafers and creating broad face electrical contacts on both sides of the wafer. Electrical contacts were created by using an AJA International DC Confocal Sputtering system to deposit a one-quarter square centimeter gold film about 150 nanometers thick onto both sides of the boron carbide sample, as well as a similar sized silicon wafer for baseline comparison. A Keithley 6437 picoammeter and DC voltage source interfaced with LabView were used for I-V analyses. Due to the safety interlock of the Keithley 6437, the current across the samples was limited to 2.5 milliamps.

For the silicon wafer, a voltage sweep from -25 volts to 25 volts, while a voltage sweep from -50 volts to 50 volts was applied to the boron carbide-silicon wafer. The current across the wafers was recorded at each of these voltage steps. This process was reported five times for both the silicon wafer and the boron carbide sample, in order to ensure repeatability and to provide a sample standard deviation. Using the generated data, current-voltage curves were created for the samples. The current-voltage characteristics of the wafers are provided in Figure 39.

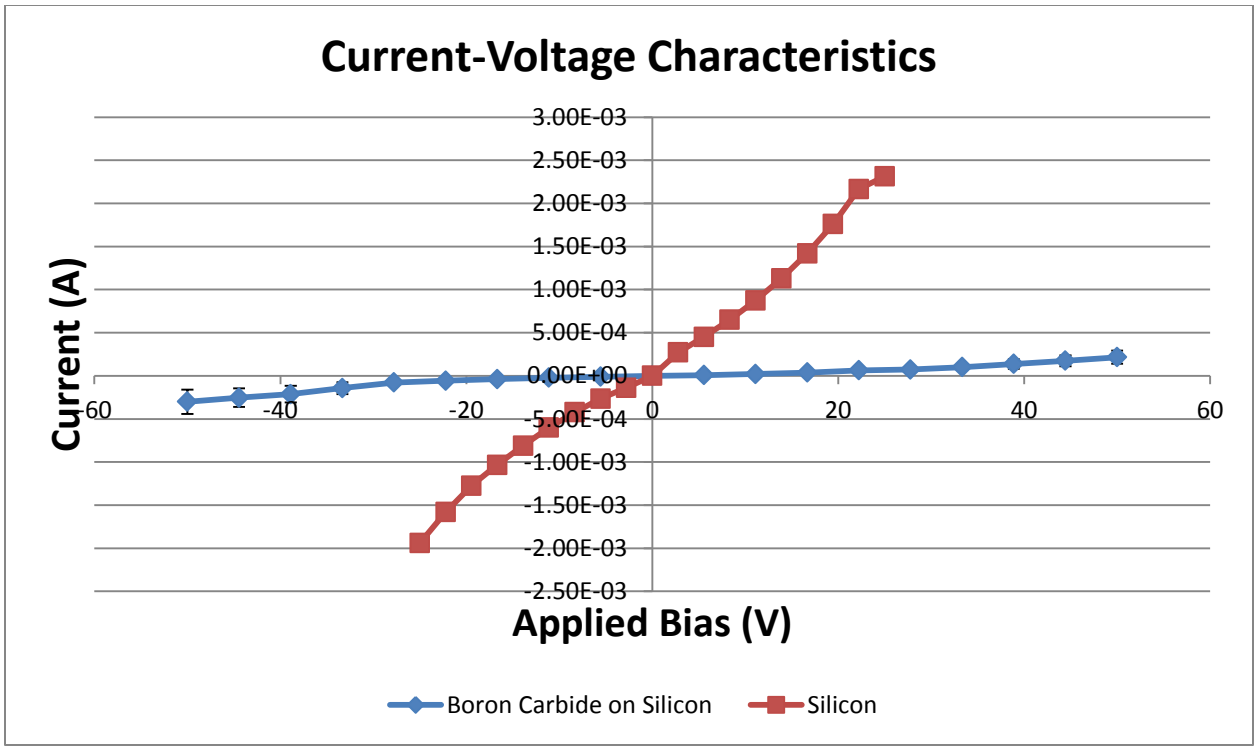

Figure 39: Current-Voltage Characteristics of Metallized Boron Carbide-Silicon Wafer and Metallized Silicon Wafer

As it can be seen, the boron carbide added a significant amount of resistance to the silicon wafers. This is ideal, since radiation detectors must be quite resistive in order to achieve a high signal-to-noise ratio [6]. However, the boron carbide-silicon sample did not demonstrate Schottky behavior, since the flow of current was not resisted in one bias direction. Rather, the measured current across the sample was proportional to the applied voltage, indicating that the device had Ohmic behavior. This Ohmic behavior is attributed to the p-n-p heterostructure created by p-type boron carbide depositing on both sides of the n-type silicon wafers. On either side of the p-n-p device, the p-type boron carbide is either forward or reverse biased. The band structure of this device permits the flow of current in both forward and reverse biasing directions [28]. This is non-ideal, since the boron carbide-silicon device must demonstrate Schottky diode behavior in order to operate as a reverse-biased p-n heterojunction capable of detecting neutrons.

Chapter 4: Conclusions and Future Work

Boron carbide films averaging 0.2 microns in thickness were deposited onto the (100) plane of seven n-type silicon wafers at an average rate of 0.07 μm/hour. The deposition was non-uniform across the surface of the silicon with a pebble-like microstructure. In addition, clusters of vertical nanowhiskers were grown atop the pebble surface. However, the elemental composition and crystallography of the vertical whiskers has yet to be determined, due to complications isolating a representative sample of the whiskers. The films were analyzed with SEM, TEM, EDS, and LIBS.

For one of the seven samples, the deposited film was scraped from the surface of the wafer onto a carbon grid TEM slide. Electron diffraction studies of the scraped boron carbide material indicated primarily polycrystalline structure, with random texturing and a few amorphous regions. For another one of the seven samples, the film composition of the pebble-like surface was composed of boron and carbon in a 2 to 1 respective ratio, as determined by LIBS. A thin sliver, called a lamella, of the boron carbide-silicon interface was then extracted from the unpolished side of a different boron carbide-silicon wafer using a FIB milling technique. It was apparent that the deposited boron carbide thin films composing the lamella were amorphous in crystal structure, as determined by electron diffraction studies. EDS determined that the elemental composition of the film was primarily boron and carbon, with some oxygen impurities.

Another of the seven samples was metallized with gold contacts on each side. The boron carbide deposition increased the resistance of the silicon wafer by one order of magnitude, from 15 kΩ to 300kΩ, as determined by current-voltage curves. This is ideal, since large electrical

resistance is an essential property of high signal-to-noise radiation detectors. The metallized sample did not demonstrate the ideal Schottky diode behavior of a p-n heterojunction. Instead, the sample exhibited Ohmic behavior, in which the electric current across the sample was proportional to the applied bias. It is hypothesized that since boron carbide was deposited on both sides of the silicon wafers, due to their orientation during growth, a p-n-p heterostructure was created. This device does not exhibit Schottky diode current-voltage characteristics.

Future work consists of analyzing the elemental composition and crystallography of the nanowhiskers that were grown; optimizing the CVD system to epitaxially grow single crystalline boron carbide onto one side of an n-type silicon wafer; conducting parametric studies on the effects of growth temperature, growth pressure, BCl_3 to CH_4 inlet gas ratio, and BCl_3 to H_2 inlet gas ratio on film deposition rates, boron carbide crystallography, and film-substrate epitaxy; creation of a boron carbide p-n heterojunction that exhibits Schottky diode behavior; conducting charge collection efficiency, transient current technique, and radiation exposure experiments on grown samples; simulating the boron carbide-silicon energy band diagram under thermal equilibrium and reverse-biased conditions; and establishing a process for characterization and optimization of doping concentrations, hole mobilities, and sheet resistances of boron carbide semiconducting thin films.

References

1. Wilkins, M.L., *Use of Boron Compounds in Lightweight Armor*, in *Boron and Refractory Borides*, V. Matkovich, Editor. 1977, Springer Berlin Heidelberg. p. 633-648.
2. Clark, H.K. and J.L. Hoard, *The Crystal Structure of Boron Carbide.* Journal of the American Chemical Society, 1943. **65**(11): p. 2115-2119.
3. Kevill, D.N., et al., *Preparation of boron-carbon compounds, including crystalline B2C material, by chemical vapor deposition.* Journal of the Less Common Metals, 1986. **117**(1–2): p. 421-425.
4. Kevill, D.N., et al., *Growth of crystals of several boron-carbon compositions by chemical vapor deposition.* Journal of Crystal Growth, 1986. **74**(1): p. 210-216.
5. Emin, D., *Structure and single-phase regime of boron carbides.* Physical Review B, 1988. **38**(9): p. 6041-6055.
6. Knoll, G.F., *Radiation Detection and Measurement*. 2010: John Wiley & Sons.
7. Jansson, U., et al., *Chemical vapour deposition of boron carbides I: Phase and chemical composition.* Thin Solid Films, 1989. **172**(1): p. 81-93.
8. Liu, Y., et al., *Uniform design and regression analysis of LPCVD boron carbide from BCl3–CH4–H2 system.* Applied Surface Science, 2009. **255**(11): p. 5729-5735.
9. Olsson, M., et al., *Chemical vapour deposition of boron carbides II: Morphology and microstructure.* Thin Solid Films, 1989. **172**(1): p. 95-109.
10. Sezer, A.O. and J.I. Brand, *Chemical vapor deposition of boron carbide.* Materials Science and Engineering: B, 2001. **79**(3): p. 191-202.
11. Vandenbulcke, L. and G. Vuillard, *Composition and structural changes of boron carbides deposited by chemical vapour deposition under various conditions of temperature and supersaturation.* Journal of the Less Common Metals, 1981. **82**(0): p. 49-56.
12. Thévenot, F., *Boron carbide—A comprehensive review.* Journal of the European Ceramic Society, 1990. **6**(4): p. 205-225.
13. Adenwalla, S., et al., *Boron carbide/n-silicon carbide heterojunction diodes.* Applied Physics Letters, 2001. **79**(26): p. 4357-4359.
14. Byun, D., et al., *Comparison of different chemical vapor deposition methodologies for the fabrication of heterojunction boron-carbide diodes.* Nanostructured Materials, 1995. **5**(4): p. 465-471.
15. Caruso, A.N., et al., *The all boron carbide diode neutron detector: Comparison with theory.* Materials Science and Engineering: B, 2006. **135**(2): p. 129-133.
16. Neamen, D.A., *Semiconductor physics and devices: basic principles*. 2003: McGraw-Hill.
17. Nina, H., et al., *Boron carbide based solid state neutron detectors: the effects of bias and time constant on detection efficiency.* Journal of Physics D: Applied Physics, 2010. **43**(27): p. 275101.
18. Aselage, T.L. and R.G. Tissot, *Lattice Constants of Boron Carbides.* Journal of the American Ceramic Society, 1992. **75**(8): p. 2207-2212.
19. Ziegler, J.F., M.D. Ziegler, and J.P. Biersack, *SRIM – The stopping and range of ions in matter (2010).* Nuclear Instruments and Methods in Physics Research Section B: Beam Interactions with Materials and Atoms, 2010. **268**(11–12): p. 1818-1823.
20. Vandenbulcke, L.G., *Theoretical and experimental studies on the chemical vapor deposition of boron carbide.* Industrial & engineering chemistry product research and development, 1985. **24**(4): p. 568-575.

21. Vepřek, S., et al., *Development of plasma CVD and feasibility study of boron carbide in-situ coatings for tokamaks.* Journal of Nuclear Materials, 1989. **162–164**(0): p. 724-731.
22. Singh, J.P. and S.N. Thakur, *Laser-Induced Breakdown Spectroscopy*. 2007: Elsevier Science.
23. Noll, R., *Laser-Induced Breakdown Spectroscopy: Fundamentals and Applications*. 2012: Springer.
24. Smith, D., *Thin-Film Deposition: Principles and Practice*. 1995: McGraw-Hill Education.
25. Reimer, L. and H. Kohl, *Transmission Electron Microscopy: Physics of Image Formation*. 2008: Springer.
26. Kramida, A., Ralchenko, Yu., Reader, J. and NIST ASD Team (2013). *NIST Atomic Spectra Database (version 5.1), [Online]*. 2013: National Institute of Standards and Technology, Gaithersburg, MD.
27. Williams, D. and C.B. Carter, *X-ray Spectrometry*, in *Transmission Electron Microscopy*. 2009, Springer US. p. 581-603.
28. Sze, S.M. and K.K. Ng, *Physics of Semiconductor Devices*. 2006: Wiley.

Vita

Thomas Wulz was born in Woodstock, GA on February 16, 1990. He attended Walker Valley High School in Cleveland, TN, where he graduated with honors. In 2008, Thomas enrolled in the University of Tennessee at Knoxville in the College of Engineering, majoring in Nuclear Engineering. During his undergraduate career, Thomas completed a 3-month internship with Tennessee Valley Authority working on project management and licensing for the Clinch River Small Modular Reactor project. He then graduated from the University of Tennessee Summa Cum Laude with his Bachelor of Science degree in Nuclear Engineering in May of 2013. Thomas then enrolled in the Graduate Program at the University of Tennessee at Knoxville in order to obtain his Master of Science degree in Nuclear Engineering. He accepted a Graduate Research Assistant position in the Nuclear Engineering Department working on Semiconductor Characterization and Thin Film Growth. Thomas graduated in May 2014 with his Master of Science and is continuing his education to obtain a PhD in Nuclear Engineering.